Study of the Wisdom-Holman Integrator for Large Time Step Simulations of Planetary Systems: Beyond Orbital Periods

Jim Rafael van der Ven
Student number: 4979524

Bachelor's Thesis in Applied Mathematics and Applied Physics

Supervised by
Dr. P. M. Visser and Prof. Dr. J. M. Thijssen

Other committee members
Dr. B. van den Dries and Prof. Dr. Y. M. Blanter

Delft University of Technology
Institute of Applied Mathematics
and
Faculty of Applied Sciences

July 31, 2025
Delft

Acknowledgements

I would like to express my deepest gratitude to my supervisors, J. M. Thijssen and especially P. M. Visser, for guiding me through the process of writing this thesis, and their patience despite the delays that occurred during the project. I would also like to thank B. van den Dries and Y. M. Blanter for taking part in the thesis committee. I am very thankful for my family, girlfriend, and friends, who kept me motivated and gave me the positive distractions when needed. Specifically, thank you to D. Willemsen, A. D. Darrell, and D. Rozenbroek for spending their time giving me feedback and tips, which I very much appreciate.

Abstract

We present an implementation of the Wisdom-Holman integrator for simulating gravitational dynamics in planetary systems: systems with one dominant central mass and N orbiting bodies, such as the Solar System. The Wisdom-Holman integrator models the motion of non-central bodies as unperturbed Kepler orbits and integrates gravitational interactions between orbiting planets as weak perturbations. Two methods to advance a body along its orbits are investigated: one using coordinate transformations (Method A) and one based on the f and g functions (Method B). Method B is shown to be significantly faster than Method A, without a significant loss of accuracy, making it the preferred method for most simulations. Simulations of the Solar System using large time steps, including time steps exceeding the orbital period of some planets, are explored to determine whether the increase in computational speed justifies the loss in accuracy. Simulations with a fixed Sun and with a dynamic Sun are considered. Results indicate that for fixed Sun simulations, while accurate simulations require small time steps, larger steps still capture the qualitative behaviour of the system. The step size of simulations with a dynamic Sun is limited by $\Delta t_{\max} = T_{\text{Mercury}}/6$. However, for small step sizes, dynamic Sun simulations accurately describe the Solar System and the restricted three-body problem in which resonance occurs. This is achieved without the use of Jacobian coordinates, which are commonly used in implementations of the Wisdom-Holman integrator. The fixed Sun and dynamic Sun simulations are shown to conserve energy, suggesting an accurate description of the system simulated.

Table 1: List of symbols and their physical meaning frequently used in this text.

Symbol	Quantity
r	radial distance
L	angular momentum
$\mathbf{r}$	position vector
$\mathbf{v}$	velocity vector
$\mathbf{p}$	momentum vector
$\mathbf{L}$	angular momentum vector
$\mathbf{z}$	combined position and momentum vector
m	mass
m_c	central body mass
m_{ci}^*	effective central body mass
μ_i	mass ratio of orbiting and central body
a	semi-major axis
b	semi-minor axis
c	linear eccentricity
l	semi-latus rectum
ϵ	eccentricity
$\boldsymbol{\epsilon}$	eccentricity vector
I	orbital inclination
Ω	longitude of ascending node
ϖ	argument of periapsis
Φ	longitude of periapsis
ν	true anomaly
E	eccentric anomaly
M	mean anomaly
λ	mean longitude
ω	mean motion
T	orbital period
τ	time at periapsis
ϕ	phase offset
t	time
t_{sim}	simulated time
Δt	time step
N	number of orbiting particles
k	current iteration
K	number of iterations
χ_i^k	quantity χ of particle i at iteration k
G	gravitational constant
$\mathcal{H}$	Hamiltonian
$\mathcal{H}_{\mathrm{Kep}}$	Kepler Hamiltonian
$\mathcal{H}_{\mathrm{pert}}$	perturbation Hamiltonian
$\mathcal{H}_{\mathrm{int}}$	interaction Hamiltonian
$\mathcal{H}_{\mathrm{cbm}}$	central body motion Hamiltonian

Contents

1 Introduction **1**

2 Theory **4**
2.1 Mathematical description of Kepler orbits 4
2.2 Kepler and Cartesian coordinate systems 6
2.2.1 From Cartesian to Kepler coordinates 7
2.2.2 From Kepler to Cartesian coordinates 9
2.3 Advancing a body along its orbit 9
2.3.1 Method A: transforming between coordinates systems 10
2.3.2 Method B: using the f and g functions 10
2.4 Gravitational interaction between orbiting bodies 10
2.4.1 Three-body system 12
2.4.2 General case with N orbiting bodies 13
2.4.3 Correcting the general case for central body motion 14
2.4.4 Special case: the two-body problem 18
2.5 The Simulation 19

3 Results and discussion **22**
3.1 Method A versus Method B 24
3.2 Error analysis 26
3.3 Perturbation magnitudes and energy conservation 30
3.4 Resonance as gauge for simulation fidelity 32

4 Conclusion **37**

References **39**

Appendix A **40**

Appendix B **41**

Appendix C **42**

1 Introduction

Two massive objects attract each other through the force of gravity. The more massive the objects, the stronger the attraction, according to Newton's law of gravity. The gravitational force also depends on the distance between the objects: it is stronger the closer the two objects are to each other — more exactly, the gravitational force is proportional to the inverse square of the distance between the objects (Murray & Dermott 2009). Gravity is too weak to notice any attraction between small masses. Here, small refers to a mass that is orders of magnitude smaller than the mass of, for example, the Earth. This is different on large scales. For instance, the gravitational attraction between the Sun and the planets in the Solar System keeps the planets in orbit around the Sun.

Being able to describe, and thus predict or reconstruct, the motion of the celestial bodies in, for example, the Solar System, is valuable, as it has many practical and scientific applications. Practical applications include the planning of space missions, for which the spacecraft's trajectory needs to be calculated accurately, and tracking and monitoring asteroids that could potentially impact the Earth. Scientific applications include research on the formation and evolution of the Solar System and the modelling of the orbits of exoplanets around their star.

The shapes of the planetary orbits in the Solar System happen to be elliptical, rather than circular. According to Kepler's laws of planetary motion, planetary orbits are, in general, elliptical, of which circular orbits are a special case (Murray & Dermott 2009). In practice, however, most orbits are at least slightly elliptical. Figure 1 shows an ellipse, with its two *focal points* represented by black dots. The Sun resides in (the vicinity of) one of these focal points, and the orbit of a planet traces out the ellipse. For many celestial bodies, especially for the eight planets in the Solar System (see Fig. 2), the orbits are more circular than the ellipse shown here.

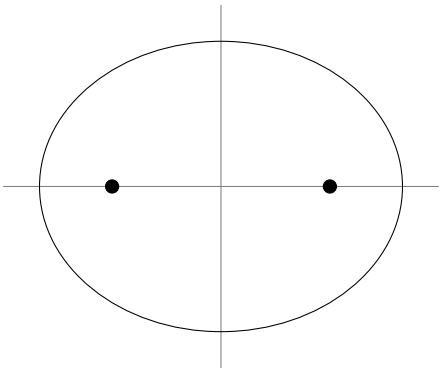

Figure 1: Ellipse. The two black dots are the focal points of the ellipse.

Kepler's laws govern the motion of one body orbiting another — or, more generally, the motion of two objects orbiting *each other*. We call these orbits *Kepler orbits*, and use this term only to refer to the elliptical orbits describing a two-body system. In this text, we focus on planetary systems: systems with a large central mass, around which an arbitrary number of small mass objects orbit. The Solar System is an example of such a system. Since there is a gravitational attraction between *any* pair of objects, there is a mutual attraction between all orbiting bodies. This attraction, although small compared to the gravitational force exerted by the central body, causes the bodies to drift off their corresponding Kepler orbits. We thus cannot describe a planetary system using Kepler's law alone, and we must resort to other methods.

A common way to study the motion of celestial bodies is by use of *simulations*. In this context, a simulation approximates the motion of a body — that is, its position and velocity — by calculating all the (gravitational) forces that are exerted on the body over a short period. With these forces known, the change in the body's position and velocity during this period can be calculated. Repeating this calculation for many periods, or *time steps*, the motion of the bodies in the system can be obtained for a longer timespan. Generally, the simulation's accuracy increases when the size of the time step decreases.

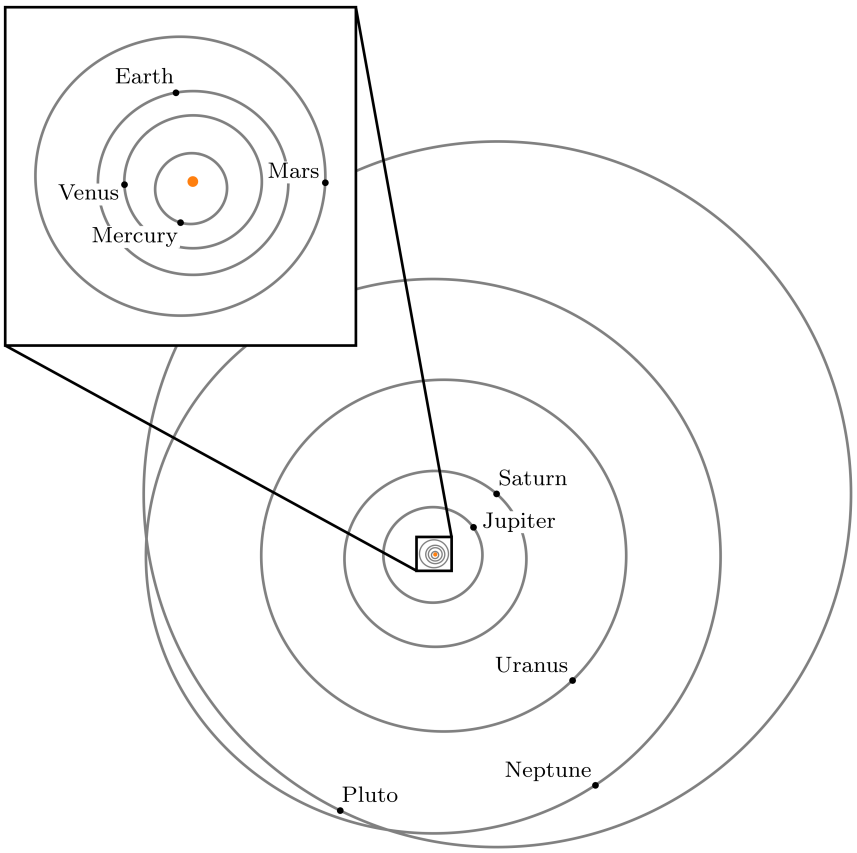

Figure 2: Orbits of the planets Mercury, Venus, Earth, Mars, Jupiter, Saturn, Uranus, Neptune and Pluto in the Solar System. The sun is shown as an orange dot, and the positions of the planets on their orbits, on the 1st of January, 2000, are shown by black dots.

The simulation method developed by Wisdom and Holman, called the Wisdom-Holman integrator, is a common way to simulate planetary systems (Wisdom & Holman 1991). Rather than directly applying numerical integration to the equations of motion, it utilises the analytical solution of unperturbed Kepler orbits for a two-body system to describe the approximate orbit of the bodies around the central body. The interactions between the orbiting bodies are modelled as weak perturbations, which cause the Kepler orbits to change slightly over time. The Wisdom-Holman integrator promises to be more accurate and faster than direct numerical integration (Wisdom & Holman 1991), partly due to larger time steps being possible. According to Viswanath (2002), to preserve numerical stability, the step size should be at most one-sixth of Mercury's orbital period for their implementation of the Wisdom-Holman integrator that models the Solar System.

We present an implementation of the Wisdom-Holman integrator and analyse to what degree the simulation produces valuable results for step sizes exceeding the limit found by Viswanath. This includes step sizes that exceed the orbital period of at least one planet in the system. We expect this may be possible due to some form of orbit averaging, which would work in the following way: the planets are in a different position along their orbits when calculating the perturbations at each iteration of the simulation (provided that a proper step size is chosen). This perturbation encompasses the interplanetary interactions during the time step, also when this time step is larger than the orbital period. This may seem inaccurate, as we only compute the perturbation at one point during the time step. However, after many iterations, this perturbation averages out because of the varying positions of the planets. The timescale of the effects of interplanetary interactions, such as the precession of the orbit, is many orders of magnitude larger than the orbital periods of planets in the Solar System. For example, the period of the precession of Earth's orbit is on the order of 10^5 y, with similar precession periods for the other planets. Therefore, we expect the perturbation term to remain minimal, also when the time step exceeds orbital periods, and we can thus apply perturbation theory in this case. While simulations with large time steps may not produce the most accurate results, they may still give valuable insight into the qualitative behaviour of a system, thus sacrificing accuracy for simulation speed.

We examine the method for two separate cases. In the first case, we assume that the central body is fixed and is thus not in motion in the chosen frame of reference. In the second case, we relax this assumption, such that the central body is in motion in the reference frame. One key difference between our implementation and the implementations presented in Wisdom & Holman (1991) and Viswanath (2002) is the lack of use of Jacobian coordinates in our case. In Jacobian coordinates, the position of body i is taken relative to the centre of mass of bodies. According to Murray & Dermott (2009), Jacobian coordinates are a necessity for a proper separation of the Hamiltonian, and thus to apply perturbation theory. However, we consider this not to be a necessity, and we think the magnitude of the perturbation Hamiltonian remains minimal without Jacobian coordinates. Hence, to decrease the number of computations, we work with standard Cartesian coordinates rather than Jacobian coordinates.

Moreover, we present two ways to advance a body along its Kepler orbit and investigate which is the more promising of the two. Method A, the more conventional method, uses rotation matrices to calculate the body's position from its orbital elements. Method B makes use of the f and g functions, which exploit the fact that the Kepler orbit lies in a plane and can thus be written as a linear combination of the position and velocity vector.

In Section 2, we begin by covering the theoretical background, which includes Kepler orbits and the Kepler and Cartesian coordinate systems that are used to describe the orbits. We then introduce the two methods to advance a body along its orbits, Method A and Method B, in Section 2.3, and we develop the perturbation theory for the time integration in Section 2.4. In Section 2.5, we outline the procedure of the simulation method. We present the results of our analysis in Section 3, first discussing the difference between Method A and Method B. We then examine the error of the simulation and test the simulation's fidelity using energy conservation and resonance. Finally, we provide the conclusion of our work in Section 4. An overview of the symbols frequently used in this text is given in Table 1 on page iv.

2 Theory

2.1 Mathematical description of Kepler orbits

The motion of a single celestial body — such as a planet, a moon, or an asteroid — orbiting around a central body due to Newtonian gravity can be described by Kepler orbits. If we place the central body at the origin, the orbit of the non-central body lies in a plane, and is described in polar coordinates (r, ν) by

$$r(\nu) = \frac{a(1-\epsilon^2)}{1+\epsilon\cos\nu}, \tag{2.1}$$

where a and ϵ are non-negative constants determining the shape of the orbit (Taylor 2005). There are four[1] types of orbits corresponding to different values of ϵ. When $\epsilon = 1$ or $\epsilon > 1$, the orbit is a parabola or a hyperbola, respectively. In these two cases, the orbit is unbounded. The more relevant case for this text is when the orbit is bounded with $0 \leq \epsilon < 1$. When $\epsilon = 0$, the orbit is a circle with radius a. When $0 < \epsilon < 1$, the orbit is an ellipse with semi-major axis a and eccentricity ϵ. In this last case, the central body is at one of the focal points of the ellipse, the main focus, as shown in Figure 3(a). We call the points on the orbit nearest to and farthest from the central body the periapsis and apoapsis, respectively, and we define the eccentricity vector $\boldsymbol{\epsilon}$ as the vector in the direction from the periapsis to apoapsis, with magnitude ϵ.

Equation (2.1) describes the orbit of a body using the angle ν, the (counterclockwise) angle between $\boldsymbol{\epsilon}$ and $\mathbf{r}$. ν is called the *true anomaly*. In many scenarios, it is more convenient to work with either the *eccentric anomaly* E or the *mean anomaly* M, which we define here. These three different anomalies all describe the body's position on the orbit. Since they use the periapsis as a reference point, which is not defined for circular orbits, these angles are only defined for elliptical orbits $(0 < \epsilon < 1)$.

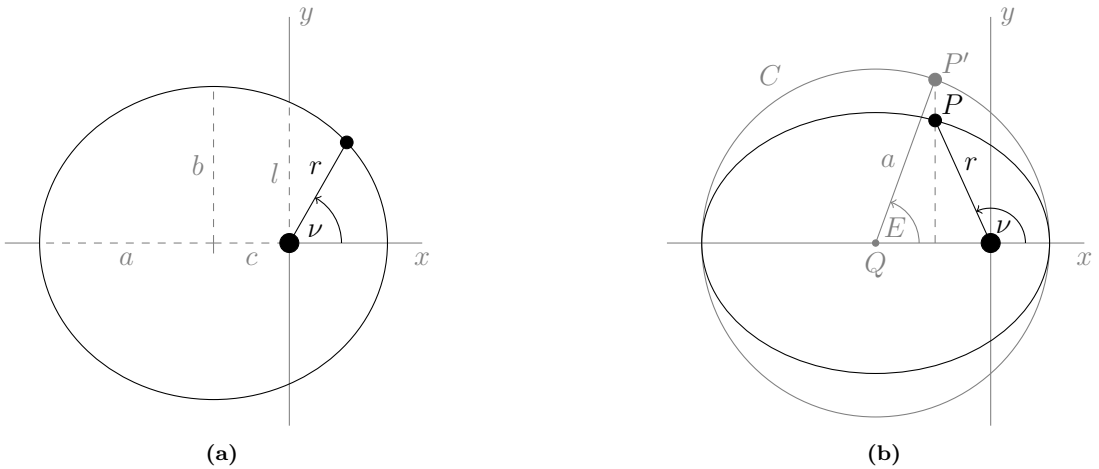

Figure 3: (a) Geometry of a body in a Kepler orbit around a central body fixed at the origin. The angle ν is the true anomaly, which is related to the distance r by Equation (2.1). The lengths a and b are the semi-major and semi-minor axes, respectively, c is the distance from the centre of the ellipse to one of its focal points, and l is the semi-latus rectum. (b) Geometry of a body, situated in point P, orbiting a central body situated at the origin, relating the eccentric anomaly E to the true anomaly ν. The eccentric anomaly is defined as the angle between the semi-major axis and the line segment QP'.

[1] Or three types when circular orbits are not considered separately from elliptical orbits.

Let C be the auxiliary circle with radius a and centre located at the same point as the centre of the ellipse, as shown in Figure 3(b). Suppose the body is at point P on the (elliptical) orbit. A line perpendicular to the semi-major axis and passing through P intersects C at some point. Call this point P'. The eccentric anomaly E is defined as the counterclockwise angle between the semi-major axis and the line segment QP' (Murray & Dermott 2009).

Recall that an ellipse with semi-major axis a and semi-minor axis b, centred at the point $(-c, 0)$, with $\boldsymbol{\epsilon}$ along the x-axis, can be described by

$$\frac{(x+c)^2}{a^2} + \frac{y^2}{b^2} = 1.$$

With the origin located at the main focus of the ellipse, we can write the position of the body as (see Fig. 3(b))

$$\begin{cases} x = a\cos E - c = a(\cos E - \epsilon) \\ y = b\sin E = a\sqrt{1-\epsilon^2}\sin E, \end{cases} \tag{2.2}$$

where $c = a\epsilon$ is the linear eccentricity, the distance from the centre of the ellipse to one of its focal points. The value of y is obtained from

$$\frac{y^2}{b^2} = 1 - \frac{(x+c)^2}{a^2} = 1 - \cos^2 E = \sin^2 E.$$

We assume the rotation is in the direction of positive ν, and thus positive E, so we take the positive solution as in Equation (2.2). From Equation (2.2), an expression for r in terms of the eccentric anomaly can be readily obtained:

$$\begin{aligned} r^2 &= a^2(\cos E - \epsilon)^2 + a^2(1-\epsilon^2)\sin^2 E \\ &= a^2\left[\cos^2 E + \epsilon^2 - 2\epsilon\cos E + \sin^2 E - \epsilon^2\sin^2 E\right] \\ &= a^2\left[1 + \epsilon^2\cos^2 E - 2\epsilon\cos E\right] \\ &= a^2\left[1 - \epsilon\cos E\right]^2, \end{aligned}$$

where we used $\sin^2 E = 1 - \cos^2 E$. Taking the square root leaves us with

$$r = a(1 - \epsilon\cos E). \tag{2.3}$$

We can get the useful relation between the eccentric anomaly and true anomaly by equating Equations (2.1) and (2.3), which, after rewriting, becomes

$$\cos\nu = \frac{\cos E - \epsilon}{1 - \epsilon\cos E}. \tag{2.4}$$

To get the eccentric anomaly directly from the position of the body, we substitute the definition of the true anomaly, $\cos\nu = \hat{\mathbf{r}}\cdot\hat{\boldsymbol{\epsilon}}$, into Equation (2.4). This yields

$$\cos E = \frac{\epsilon + \hat{\mathbf{r}}\cdot\hat{\boldsymbol{\epsilon}}}{1 + \epsilon\,(\hat{\mathbf{r}}\cdot\hat{\boldsymbol{\epsilon}})} = \frac{\epsilon + \hat{\mathbf{r}}\cdot\hat{\boldsymbol{\epsilon}}}{1 + \hat{\mathbf{r}}\cdot\boldsymbol{\epsilon}}. \tag{2.5}$$

Solving for E in Equation (2.5) using the inverse cosine results in the smallest angle between $\boldsymbol{\epsilon}$ and $\mathbf{r}$ rather than the counterclockwise angle. However, we can use the cross product between the two vectors to determine the relative orientation and calculate the right angle accordingly.

A downside of the true or eccentric anomaly is that they do not change linearly in time. Let ω be the mean motion of the body, that is,

$$\omega := \frac{2\pi}{T},$$

with T the period of the orbit, and let τ be the time at which the body crosses the periapsis. We now define the mean anomaly M as

$$M := \omega(t - \tau) = \omega t + \phi. \tag{2.6}$$

Here $\phi = -\omega\tau$ is the phase offset. Hence, contrary to the true and eccentric anomaly, the mean anomaly is linear in time. The relation between M and E is known as Kepler's equation and is given by (Murray & Dermott 2009)

$$M = E - \epsilon \sin E. \tag{2.7}$$

Kepler's equation is transcendental in E. Hence, if we want to solve for the eccentric anomaly, we have to resort to iterative methods such as the Newton-Raphson method.

During each time step of the simulation, a body moves along its Kepler orbit. To know its position and velocity after some time step Δt, it is required to know how the eccentric anomaly changes over time. One way we can achieve this is to increase the mean anomaly M^0 to $M^1 = M^0 + \Delta M = M^0 + \omega\Delta t$, and calculate the new eccentric anomaly E^1 from M^1 using Kepler's equation (Eq. (2.7)). This can be done by (numerically) solving for E^1 in

$$\omega\Delta t = (E^1 - E^0) - \epsilon(\sin E^1 - \sin E^0). \tag{2.8}$$

However, since the periapsis is not well defined for $\epsilon = 0$, neither are E and ϕ. This means Equation (2.8) might not be ideal to calculate E^1 from E^0 for small values of ϵ, as it could lead to significant numerical errors. Nevertheless, the difference $\Delta E = E^1 - E^0$ is well defined, regardless of the value of ϵ. Hence, we introduce the formula

$$\omega\Delta t - \Delta E = (1 - \cos\Delta E)\,\frac{\mathbf{r}^0 \cdot \mathbf{v}^0}{\omega a^2} - \left(1 - \frac{r^0}{a}\right)\sin\Delta E, \tag{2.9}$$

which is derived in Appendix B. The formula does not make direct use of either E^1 or E^0. Since $\mathbf{r}^0$ and $\mathbf{v}^0$ are perpendicular for circular orbits, we have that $\mathbf{r}^0 \cdot \mathbf{v}^0 \to 0$ whenever $\epsilon \to 0$. Moreover, in this case we have that $r^0 \to a$ by Equation (2.1). According to Equation (2.9), we thus have that $\Delta E \to \omega\Delta t$ in this circular orbit limit, and we conclude that the formula is well-behaved for small eccentricities.

2.2 Kepler and Cartesian coordinate systems

Up to this point, we have limited ourselves to the situation where the elliptical orbit is in the xy-plane. With more than one non-central body, however, this is not possible as the bodies could be located anywhere around the central body. In this section, we generalise the situation to three dimensions, and it is convenient to work with two separate

coordinate systems in which the particle state can be described: the Cartesian coordinates and the Kepler coordinates. The particle state in Cartesian coordinates is given by the position and velocity vector pair $(\mathbf{r}, \mathbf{v})$ or, more specifically, by

$$(x,\ y,\ z,\ v_x,\ v_y,\ v_z). \tag{2.10}$$

In the Kepler coordinates, the state is

$$(a,\ \epsilon,\ \phi,\ I,\ \Omega,\ \varpi). \tag{2.11}$$

The first three variables in (2.11) have been introduced in Section 2.1. The inclination I is the angle the orbital plane makes with the reference plane, which is taken to be the xy-plane (see Fig. 4). The longitude of the ascending node Ω is the angle between the x-axis and the ascending node, the point at which the body moves through the reference plane in the positive z-direction. Define the vector

$$\mathbf{n} := \mathbf{k} \times \mathbf{L}, \tag{2.12}$$

where $\mathbf{k}$ is the unit vector pointing in the z-direction, and $\mathbf{L} = m\mathbf{r} \times \mathbf{v}$ is the orbital angular momentum of the particle. The vector $\mathbf{n}$ points from the centre of the ellipse to the ascending node, and we define the argument of periapsis ϖ as the counterclockwise angle between $\mathbf{n}$ and $\boldsymbol{\epsilon}$. For later reference, we also introduce the longitude of periapsis Φ and the mean longitude λ. The longitude of periapsis is defined as

$$\Phi := \varpi + \Omega. \tag{2.13}$$

If $I = 0$, Φ is just the polar angle (as measured from the x-axis) of the periapsis. Using the longitude of periapsis, we define the mean longitude as

$$\lambda := M + \Phi, \tag{2.14}$$

which is the polar angle of the position vector for the case where both $\epsilon = 0$ and $I = 0$.

Note that the variables in the Cartesian coordinate system change over time while the body is orbiting the central body, but the variables in the Kepler coordinates are constant — provided that the body is unperturbed. This means we need the time t to change between coordinate systems. We will next illustrate how to do this.

2.2.1 From Cartesian to Kepler coordinates

Suppose that the particle is described by the Cartesian coordinate system as in (2.10). We want to describe the particle by its Kepler coordinates — that is, we want to know the values of the variables given by (2.11). We first calculate the angular momentum, $\mathbf{L} = m\mathbf{r} \times \mathbf{v}$, from which we calculate the eccentricity vector using

$$\boldsymbol{\epsilon} = \frac{\mathbf{v} \times \mathbf{L}}{Gm_c m} - \frac{\mathbf{r}}{r}, \tag{2.15}$$

where G is the gravitational constant, m_c is the mass of the central body, and m is the particle mass (Visser 2023). One can prove this formula by taking the dot product with $\mathbf{r}$ on both sides of the equation, using the fact that $\mathbf{r} \cdot (\mathbf{v} \times \mathbf{L}) = \mathbf{L} \cdot (\mathbf{r} \times \mathbf{v}) = L^2/m$, and finally recovering Equation (2.1). The semi-major axis is given by

$$a = \frac{l}{1 - \epsilon^2}, \tag{2.16}$$

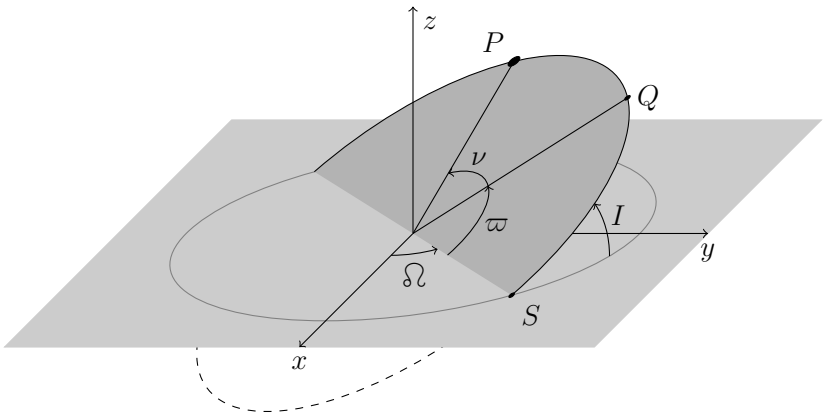

Figure 4: Orientation of a celestial body (situated in point P) in three dimensions. The inclination I is the angle the orbital plane makes with the plane of reference (the xy-plane shown in light grey). The longitude of the ascending node $\☊$ is the angle between the x-axis and the ascending node, the point at which the body moves through the plane of reference in the positive z-direction (point S). The argument of periapsis ϖ is the angle measured from the ascending node to the periapsis (point Q). As before, the angle ν is the true anomaly.

where l, defined as[2]

$$l = \frac{L^2}{Gm_c m^2},$$

is the semi-latus rectum (Taylor 2005). The geometrical meaning of the semi-latus rectum is depicted in Figure 3(a). The inclination is calculated readily using its definition given above, and by observing that the angle between the orbital plane and the xy-plane is the same as the angle between the angular momentum vector and the (positive) z-axis. Hence,

$$I = \arccos \frac{\mathbf{L} \cdot \mathbf{k}}{|\mathbf{L}|\,|\mathbf{k}|} = \arccos \frac{L_z}{L}.$$

To determine $\☊$, we first calculate

$$\☊' = \arccos \frac{n_x}{|\mathbf{n}|}, \tag{2.17}$$

with $\mathbf{n}$ as given in Equation (2.12). We obtain the longitude of the ascending node from

$$\☊ = \begin{cases} \☊' & \text{for } n_y \geq 0, \\ 2\pi - \☊' & \text{for } n_y < 0. \end{cases}$$

Similarly, we calculate

$$\varpi' = \arccos \frac{\mathbf{n} \cdot \boldsymbol{\epsilon}}{|\mathbf{n}|\,|\boldsymbol{\epsilon}|}, \tag{2.18}$$

such that the argument of periapsis is given by

$$\varpi = \begin{cases} \varpi' & \text{for } \epsilon_z \geq 0, \\ 2\pi - \varpi' & \text{for } \epsilon_z < 0. \end{cases}$$

[2]To be exact, for a two-body system $l = L^2/(Gm_c m\tilde{\mu})$, where $\tilde{\mu} = m_c m/(m_c + m)$ is the reduced mass. In this model, the motion of the central body is also taken into consideration. However, in this text we have $m_c \gg m$ and in that case $\tilde{\mu} \approx m$. For a system with more than two particles, a method to model the motion of the central body is discussed in Sections 2.4.3 and 2.4.4.

From Equation (2.18), we can see that, as explained in Section 2.1, the argument of periapsis is not defined for $\epsilon = 0$. Lastly, we obtain the phase offset ϕ from Equations (2.5) – (2.7).

2.2.2 From Kepler to Cartesian coordinates

The reverse situation, where we need to obtain the Cartesian state $(\mathbf{r}, \mathbf{v})$ from the Kepler state $(a, \epsilon, \phi, I, \Omega, \varpi)$ is more straightforward. We first calculate the mean motion of the body by employing Kepler's third law (Murray & Dermott 2009),

$$\omega = \sqrt{\frac{Gm_c}{a^3}}, \tag{2.19}$$

and we define the rotation matrix $\mathscr{R}$ by

$$\mathscr{R} := \begin{pmatrix} \cos\Omega & -\sin\Omega & 0 \\ \sin\Omega & \cos\Omega & 0 \\ 0 & 0 & 1 \end{pmatrix} \begin{pmatrix} 1 & 0 & 0 \\ 0 & \cos I & -\sin I \\ 0 & \sin I & \cos I \end{pmatrix} \begin{pmatrix} \cos\varpi & -\sin\varpi & 0 \\ \sin\varpi & \cos\varpi & 0 \\ 0 & 0 & 1 \end{pmatrix}.$$

We obtain E from Equations (2.6) and (2.7) and so, by Equation (2.2),

$$\mathbf{r} = \mathscr{R} \begin{pmatrix} a\cos E - c \\ b\sin E \\ 0 \end{pmatrix}. \tag{2.20}$$

For the velocity vector, we need to know the time derivative of E. By differentiating Kepler's equation,

$$M = \omega(t - \tau) = E - \epsilon \sin E,$$

with respect to time[3], it follows that

$$\frac{\mathrm{d}E}{\mathrm{d}t} = \frac{\omega}{1 - \epsilon\cos E} = \frac{\omega a}{r}, \tag{2.21}$$

where we used Equation (2.3). It follows that

$$\mathbf{v} = \frac{\omega a}{r} \mathscr{R} \begin{pmatrix} -a\sin E \\ b\cos E \\ 0 \end{pmatrix}. \tag{2.22}$$

2.3 Advancing a body along its orbit

While running the simulation using the Wisdom-Holman integrator, the body has to be advanced along its Kepler orbit every iteration. We present two methods to do this. The first method utilises the rotation matrix, changing between the Cartesian and Kepler coordinates each iteration. The second method is based on the so-called f and g functions, and essentially remains in the Cartesian coordinate system. Note that interaction between orbiting bodies is not yet accounted for here, and the orbits of the bodies are still described solely by Kepler's laws.

[3]It should be noted that, strictly speaking, this is incorrect, as Kepler's equation is derived in Murray & Dermott (2009) by first calculating $\mathrm{d}E/\mathrm{d}t$ by other means and then integrating it, making the argument given here circular. However, it is possible to derive Kepler's equation directly using a geometrical argument as described in, for example, Visser (2023).

2.3.1 Method A: transforming between coordinates systems

Suppose we know the particle state $(\mathbf{r}^0, \mathbf{v}^0)$ and we want to advance the particle along its orbit during a time Δt — that is, we want to know the particle state $(\mathbf{r}^1, \mathbf{v}^1)$ after a time Δt. We first convert to Kepler coordinates as described in Section 2.2.1 (retrieving ϕ is not necessary here — invoking Equation (2.5) to obtain E^0 suffices). We obtain the mean anomaly M^0 using Kepler's equation, and we increment its value by $\Delta M = \omega \Delta t$ to M^1. Again using Kepler's equation, we recover the new value of the eccentric anomaly E^1 (one could also use Equation (2.8) to obtain E^1 more directly). Finally, by invoking Equations (2.20) and (2.22) we can find $\mathbf{r}^1$ and $\mathbf{v}^1$.

2.3.2 Method B: using the f and g functions

An alternative way to advance the particle is by using the f and g functions, which are described in Appendix A. Suppose again that the particle is in the state $(\mathbf{r}^0, \mathbf{v}^0)$, and we want to know the state $(\mathbf{r}^1, \mathbf{v}^1)$ after time step Δt. As the orbit lies in a plane, and since this plane is spanned by the vectors $\mathbf{r}^0$ and $\mathbf{v}^0$, we write (Murray & Dermott 2009)

$$\mathbf{r}^1 = f(\Delta t)\mathbf{r}^0 + g(\Delta t)\mathbf{v}^0 \tag{2.23}$$

and

$$\mathbf{v}^1 = \dot{f}(\Delta t)\mathbf{r}^0 + \dot{g}(\Delta t)\mathbf{v}^0. \tag{2.24}$$

The formulas for f, g, $\dot{f}$ and $\dot{g}$ are given by Equations (A.4) – (A.7). f and g depend on time only through Δt and ΔE. We can find ΔE in the same way as in Method A ($\Delta E = E^1 - E^0$) and compute $\mathbf{r}^1$ and $\mathbf{v}^1$ accordingly. However, as discussed at the end of Section 2.1, when ϵ is small, calculating ΔE in this manner may result in significant numerical errors. This presents a potential advantage of Method B over Method A, since we can use Equation (2.9) to obtain ΔE directly. Another advantage of Method B is that it is likely faster than Method A, as the number of calculations that must be performed is significantly smaller for Method B compared to Method A.

2.4 Gravitational interaction between orbiting bodies

In the preceding sections, we assumed that there were only two bodies in the system. In general, planetary systems contain many more bodies that each influence each other gravitationally. We model such a system, i.e. a system with one central body that contains most — over 99% in the case of the Solar System — of the total mass in the system, by assuming that all bodies are in a Kepler orbit around the central body. The interactions between all non-central bodies are modelled as (weak) perturbations that change the geometry of the orbits over time. Mathematically, this means the values of the orbital elements in (2.11) do change over time, contrary to a two-body system that we considered before.

To this end, we split the Hamiltonian of the entire system,

$$\mathcal{H} = E_{\text{kin}} + E_{\text{pot}},$$

with E_{kin} the kinetic energy and E_{pot} the potential energy, into a Kepler part and a perturbation part as

$$\mathcal{H} = \mathcal{H}_{\text{Kep}} + \mathcal{H}_{\text{pert}}. \tag{2.25}$$

The Kepler Hamiltonian for a single orbiting particle with mass m, radial distance $r = |\mathbf{r}|$ and momentum $p = |\mathbf{p}|$, is of the form

$$\mathcal{H}_{\text{Kep}} = \frac{p^2}{2m} - \frac{Gm_c m}{r},$$

which is the sum of its kinetic energy and the gravitational potential energy due to the central body. Using Hamilton's equations,

$$\dot{\mathbf{r}} = \frac{\partial \mathcal{H}}{\partial \mathbf{p}} \quad \text{and} \quad \dot{\mathbf{p}} = -\frac{\partial \mathcal{H}}{\partial \mathbf{r}},$$

the exact solution of the orbit can be derived, and is given by Equation (2.1). We define the matrix

$$J = \begin{pmatrix} 0 & I \\ -I & 0 \end{pmatrix},$$

where I is the 3×3 identity matrix, and for each particle we define the state vector $\mathbf{z} := (\mathbf{r}, \mathbf{p}) \in \mathbb{R}^6$. We can now write Hamilton's equations as (Thijsen 2007)

$$\dot{\mathbf{z}} = J\nabla\mathcal{H}(\mathbf{z}),$$

where

$$\nabla\mathcal{H} = \left(\frac{\partial \mathcal{H}}{\partial \mathbf{r}}, \frac{\partial \mathcal{H}}{\partial \mathbf{p}}\right).$$

We want to calculate the body's position and momentum at time t^1 when its position at t^0 is known. We achieve this in the following way. The splitting in Equation (2.25) yields

$$\begin{aligned}
\mathbf{z}(t^1) &= \mathbf{z}(t^0) + \int_{t^0}^{t^1} \dot{\mathbf{z}}(t)\mathrm{d}t \\
&= \mathbf{z}(t^0) + \int_{t^0}^{t^1} J\nabla\mathcal{H}(\mathbf{z}(t))\mathrm{d}t \\
&= \mathbf{z}(t^0) + \int_{t^0}^{t^1} J\nabla\mathcal{H}_{\text{Kep}}(\mathbf{z}(t))\mathrm{d}t + \int_{t^0}^{t^1} J\nabla\mathcal{H}_{\text{pert}}(\mathbf{z}(t))\mathrm{d}t. \qquad (2.26)
\end{aligned}$$

Let $\mathbf{z}_{\text{Kep}}(t^0, t^1)$ be the state vector at time t^1 for an unperturbed particle when the state vector at time t^0 is known. We can write this as

$$\mathbf{z}_{\text{Kep}}(t^0, t^1) = \mathbf{z}(t^0) + \int_{t^0}^{t^1} J\nabla\mathcal{H}_{\text{Kep}}(\mathbf{z}_{\text{Kep}}(t^0, t))\mathrm{d}t.$$

For this scenario, the exact solution can be obtained and is given in terms of Kepler orbits. We approximate Equation (2.26) by

$$\begin{aligned}
\mathbf{z}(t^1) &\approx \mathbf{z}_{\text{Kep}}(t^0, t^1) + \int_{t^0}^{t^1} J\nabla\mathcal{H}_{\text{pert}}(\mathbf{z}_{\text{Kep}}(t^0, t))\mathrm{d}t \qquad (2.27) \\
&\approx \mathbf{z}_{\text{Kep}}(t^0, t^1) + J\nabla\mathcal{H}_{\text{pert}}(\mathbf{z})|_{\mathbf{z}=\mathbf{z}_{\text{Kep}}(t^0,t^1)}\,\Delta t \\
&= \mathbf{z}_{\text{Kep}}(t^0, t^1) + \dot{\mathbf{z}}_{\text{pert}}|_{\mathbf{z}=\mathbf{z}_{\text{Kep}}(t^0,t^1)}\,\Delta t, \qquad (2.28)
\end{aligned}$$

where we substituted $\mathbf{z}_{\text{Kep}}(t^0, t)$ for $\mathbf{z}(t)$ in Equation (2.26) and approximated the second integral by the product of the value of the integrand at t^1 and the time step $\Delta t = t^1 - t^0$. It remains to find $\dot{\mathbf{z}}_{\text{pert}} := J\nabla\mathcal{H}_{\text{pert}}(\mathbf{z})$ for each body in the system.

2.4.1 Three-body system

We now consider a simplified model of two bodies orbiting a fixed central body. In the following sections, we generalise this to the case with N orbiting bodies, and to the case with N orbiting bodies where the central body is not fixed at the origin.

Assume body A and B are in a Kepler orbit around the central body, and thus influence each other gravitationally. The Hamiltonian of the entire system is given by

$$\begin{aligned}\mathcal{H}(\mathbf{z}_A, \mathbf{z}_B) &= \underbrace{\left(\frac{p_A^2}{2m_A} + \frac{p_B^2}{2m_B}\right)}_{E_{\text{kin}}} + \underbrace{\left(-\frac{Gm_cm_A}{|\mathbf{r}_A|} - \frac{Gm_cm_B}{|\mathbf{r}_B|} - \frac{Gm_Am_B}{|\mathbf{r}_A - \mathbf{r}_B|}\right)}_{E_{\text{pot}}} \\ &= \underbrace{\left(\frac{p_A^2}{2m_A} - \frac{Gm_cm_A}{|\mathbf{r}_A|}\right) + \left(\frac{p_B^2}{2m_B} - \frac{Gm_cm_B}{|\mathbf{r}_B|}\right)}_{\mathcal{H}_{\text{Kep}}} + \underbrace{\left(-\frac{Gm_Am_B}{|\mathbf{r}_A - \mathbf{r}_B|}\right)}_{\mathcal{H}_{\text{int}}},\end{aligned}$$

where $\mathbf{z}_i$ denotes the combined position and momentum vector of body i defined in Section 2.4. Observe that the coordinates of the central body are not dynamical degrees of freedom by the assumption that it is fixed, so it does not contribute to the Hamiltonian. We split the Hamiltonian according to Equation (2.25) as the sum of the Kepler Hamiltonian,

$$\mathcal{H}_{\text{Kep}} = \left(\frac{p_A^2}{2m_A} - \frac{Gm_cm_A}{|\mathbf{r}_A|}\right) + \left(\frac{p_B^2}{2m_B} - \frac{Gm_cm_B}{|\mathbf{r}_B|}\right),$$

and the perturbation Hamiltonian, which we call the interaction Hamiltonian $\mathcal{H}_{\text{int}}$, as it models the mutual gravitational interaction between the non-central particles,

$$\mathcal{H}_{\text{pert}} = \mathcal{H}_{\text{int}} = -\frac{Gm_Am_B}{|\mathbf{r}_A - \mathbf{r}_B|}.$$

We thus have that $\mathcal{H} = \mathcal{H}_{\text{Kep}} + \mathcal{H}_{\text{int}}$. As explained above, $\mathcal{H}_{\text{Kep}}$ is the Hamiltonian for the (separate) Kepler orbits of bodies A and B. To calculate $(\dot{\mathbf{z}}_A)_{\text{pert}}$, we apply Hamilton's equations for body A to the perturbation Hamiltonian. As $\mathcal{H}_{\text{int}}$ is independent of $\mathbf{p}_A$, the first Hamilton equation gives $(\dot{\mathbf{r}}_A)_{\text{pert}} = \mathbf{0}$. According to Equation (2.28), we have that $\mathbf{r}_A(t^1) \approx (\mathbf{r}_A)_{\text{Kep}}(t^0, t^1)$. Analogously, $\mathbf{r}_B(t^1) \approx (\mathbf{r}_B)_{\text{Kep}}(t^0, t^1)$. The second Hamilton equation results in

$$(\dot{\mathbf{p}}_A)_{\text{pert}} = -\frac{\partial \mathcal{H}_{\text{pert}}}{\partial \mathbf{r}_A} = -\frac{Gm_Am_B}{|\mathbf{r}_A - \mathbf{r}_B|^3}(\mathbf{r}_A - \mathbf{r}_B),$$

from which it follows that

$$(\dot{\mathbf{v}}_A)_{\text{pert}} = -\frac{Gm_B}{|\mathbf{r}_A - \mathbf{r}_B|^3}(\mathbf{r}_A - \mathbf{r}_B).$$

Combining this with Equation (2.28), we get

$$\mathbf{v}_i(t^1) \approx (\mathbf{v}_i)_{\text{Kep}}(t^0, t^1) - \frac{Gm_B}{|\mathbf{r}_A(t^1) - \mathbf{r}_B(t^1)|^3}(\mathbf{r}_A(t^1) - \mathbf{r}_B(t^1))\Delta t,$$

with an analogous result for $(\dot{\mathbf{v}}_B)_{\text{pert}}$.

2.4.2 General case with N orbiting bodies

For the general case with N orbiting bodies (with the central body still fixed at the origin), the procedure is analogous to the one with two orbiting bodies. In this case, the Hamiltonian of the system is given by

$$\mathcal{H}(\mathbf{z}_1, \ldots, \mathbf{z}_N) = \sum_{i=1}^{N} \left(\frac{p_i^2}{2m_i} - \frac{Gm_c m_i}{|\mathbf{r}_i|} \right) - \sum_{i=1}^{N} \sum_{j=i+1}^{N} \frac{Gm_i m_j}{|\mathbf{r}_i - \mathbf{r}_j|}.$$

As before, we split the Hamiltonian into two parts. The Kepler part is now given by

$$\mathcal{H}_{\text{Kep}} = \sum_{i=1}^{N} \left(\frac{p_i^2}{2m_i} - \frac{Gm_c m_i}{|\mathbf{r}_i|} \right), \tag{2.29}$$

and the perturbation part is

$$\mathcal{H}_{\text{pert}} = \mathcal{H}_{\text{int}} = -\sum_{i=1}^{N} \sum_{j=i+1}^{N} \frac{Gm_i m_j}{|\mathbf{r}_i - \mathbf{r}_j|}. \tag{2.30}$$

Define the *particle* Kepler and interaction Hamiltonian, $(\mathcal{H}_i)_{\text{Kep}}$ and $(\mathcal{H}_i)_{\text{int}}$, for each particle i by

$$(\mathcal{H}_i)_{\text{Kep}} = \frac{p_i^2}{2m_i} - \frac{Gm_c m_i}{|\mathbf{r}_i|},$$

and

$$(\mathcal{H}_i)_{\text{int}} = -\sum_{j \neq i}^{N} \frac{Gm_i m_j}{|\mathbf{r}_i - \mathbf{r}_j|}. \tag{2.31}$$

Observe that the $(\mathcal{H}_i)_{\text{Kep}}$ are simply the terms in the sum in Equation (2.29), but this is not the case for the $(\mathcal{H}_i)_{\text{int}}$ in Equation (2.30) due to double counting. We can get an insight into the relative size of the perturbation by calculating the ratio $|(\mathcal{H}_i)_{\text{int}}/(\mathcal{H}_i)_{\text{Kep}}|$. The Kepler Hamiltonian is the total energy of an unperturbed body in a Kepler orbit. Hence,

$$(\mathcal{H}_i)_{\text{Kep}} = (E_i)_{\text{Kep}} = \frac{p_i^2}{2m_i} - \frac{Gm_c m_i}{r_i} = -\frac{Gm_c m_i}{2a_i}, \tag{2.32}$$

with a_i the semi-major axis (Murray & Dermott 2009). We therefore have

$$\begin{aligned} \left| \frac{(\mathcal{H}_i)_{\text{int}}}{(\mathcal{H}_i)_{\text{Kep}}} \right| &\approx (N-1) \left(\frac{Gm_i \overline{m}_{iN}}{\overline{r}_{iN}} \right) \left(\frac{2a_i}{Gm_c m_i} \right) \\ &= 2(N-1) \frac{\overline{m}_{iN}}{m_c} \frac{a_i}{\overline{r}_{iN}} \approx 2(N-1) \frac{\overline{m}_{iN}}{m_c}. \end{aligned} \tag{2.33}$$

Here, $\overline{m}_{iN}$ is the average mass of the non-central bodies excluding body i and $\overline{r}_{iN}$ is the average distance from body i to the other non-central bodies. The factor $N-1$ is included because of the sum in Equation (2.31). The last approximation comes from the fact that a_i and $\overline{r}_{iN}$ have roughly the same order of magnitude. By the assumption that $m_i \ll m_c$ for $i = 1, \ldots, N$, and thus also $\overline{m}_{iN} \ll m_c$, we conclude that $|(\mathcal{H}_i)_{\text{int}}| \ll |(\mathcal{H}_i)_{\text{Kep}}|$. For instance, $m_{\text{Earth}}/m_{\text{Sun}} \approx 3 \cdot 10^{-6}$ (See Table 2). One might consider the case where N is large enough such that the inequality does not hold any more. However, m_c is generally

Table 2: Rough approximation of the mass m in kg and the radial distance $r = |\mathbf{r}|$ in AU (1 AU $= 150 \cdot 10^9$ m) for some bodies in the Solar System (Murray & Dermott 2009). Fixing the centre of mass in the origin, and because of Jupiter's large mass, we have $r_{\text{Sun}} \approx r_{\text{Jupiter}}(m_{\text{Jupiter}}/m_{\text{Sun}})$.

Celestial body	Mass (10^{24} kg)	Radial distance (AU)
Sun	$2 \cdot 10^6$	$5 \cdot 10^{-3}$
Mercury	$3 \cdot 10^{-1}$	$4 \cdot 10^{-1}$
Earth	6	1
Jupiter	$2 \cdot 10^3$	5
Neptune	$1 \cdot 10^2$	$3 \cdot 10^1$

several orders of magnitude larger than m_i, so this is only a concern when simulating systems with a large number of particles.

We again use Hamilton's equations in combination with Equation (2.30) to obtain $(\dot{\mathbf{r}}_i)_{\text{pert}}$ and $(\dot{\mathbf{v}}_i)_{\text{pert}}$. The first Hamilton equation results in $(\dot{\mathbf{r}}_i)_{\text{pert}} = \mathbf{0}$ for all $i = 1, \ldots, N$. The second yields

$$(\dot{\mathbf{v}}_i)_{\text{pert}} = -\frac{1}{m_i}\frac{\partial \mathcal{H}_{\text{pert}}}{\partial \mathbf{r}_i} = -\sum_{j \neq i} \frac{Gm_j}{|\mathbf{r}_i - \mathbf{r}_j|^3}(\mathbf{r}_i - \mathbf{r}_j). \tag{2.34}$$

Substituting these results into Equation (2.28) results in

$$\mathbf{r}_i(t^1) \approx (\mathbf{r}_i)_{\text{Kep}}(t^0, t^1), \tag{2.35}$$

and

$$\mathbf{v}_i(t^1) \approx (\mathbf{v}_i)_{\text{Kep}}(t^0, t^1) - \sum_{j \neq i} \frac{Gm_j}{|\mathbf{r}_i(t^1) - \mathbf{r}_j(t^1)|^3}(\mathbf{r}_i(t^1) - \mathbf{r}_j(t^1))\Delta t. \tag{2.36}$$

These two equations are used for the numerical time integration for the simulation, where the $\mathbf{r}_j(t^1)$ in Equation (2.36) are approximated by Equation (2.35).

2.4.3 Correcting the general case for central body motion

Up to this point, we have assumed that the central body is fixed at the origin and does not move. However, this approximation might not suffice for some scenarios, for instance, when a particle is relatively close to the central body. In this section, we relax this assumption, and we assume the central body has a time-dependent position $\mathbf{r}_c$ and momentum $\mathbf{p}_c$. Because of the central body's large mass, we assume that the central body's deviation from the origin is small compared to that of the other bodies, that is $r_c \ll r_i$ for all $i = 1 \ldots N$. In Table 2, the approximate values of the mass m and radial distance $r = |\mathbf{r}|$ are given. Fixing the centre of mass in the origin, and because of Jupiter's large mass, we have $r_{\text{Sun}} \approx r_{\text{Jupiter}}(m_{\text{Jupiter}}/m_{\text{Sun}})$.

The Hamiltonian of the entire system is now given by

$$\begin{aligned}\mathcal{H}(\mathbf{z}_1,\ldots,\mathbf{z}_N,\mathbf{z}_c) &= \frac{p_c^2}{2m_c} + \sum_{i=1}^{N}\left(\frac{p_i^2}{2m_i} - \frac{Gm_cm_i}{|\mathbf{r}_i-\mathbf{r}_c|}\right) - \sum_{i=1}^{N}\sum_{j=i+1}^{N}\frac{Gm_im_j}{|\mathbf{r}_i-\mathbf{r}_j|} \\ &= \frac{p_c^2}{2m_c} + \underbrace{\sum_{i=1}^{N}\left(\frac{p_i^2}{2m_i} - \frac{Gm_cm_i}{|\mathbf{r}_i|}\right)}_{\mathcal{H}_{\text{Kep}}} \\ &\quad + \underbrace{\sum_{i=1}^{N}\left(\frac{Gm_cm_i}{|\mathbf{r}_i|} - \frac{Gm_cm_i}{|\mathbf{r}_i-\mathbf{r}_c|}\right)}_{\mathcal{H}_{\text{cbm}}} + \underbrace{\left[-\sum_{i=1}^{N}\sum_{j=i+1}^{N}\frac{Gm_im_j}{|\mathbf{r}_i-\mathbf{r}_j|}\right]}_{\mathcal{H}_{\text{int}}}. \quad (2.37)\end{aligned}$$

The Kepler Hamiltonian is given by Equation (2.29), but the perturbation part now becomes

$$\mathcal{H}_{\text{pert}} = \frac{p_c^2}{2m_c} + \mathcal{H}_{\text{int}} + \mathcal{H}_{\text{cbm}}, \quad (2.38)$$

where $\mathcal{H}_{\text{int}}$ is the interaction Hamiltonian defined in Equation (2.30), and

$$\mathcal{H}_{\text{cbm}} = \sum_{i=1}^{N}\left(\frac{Gm_cm_i}{|\mathbf{r}_i|} - \frac{Gm_cm_i}{|\mathbf{r}_i-\mathbf{r}_c|}\right) = \sum_{i=1}^{N}(\mathcal{H}_i)_{\text{cbm}} \quad (2.39)$$

is the term in the Hamiltonian due to the central body motion. Here, we have introduced

$$(\mathcal{H}_i)_{\text{cbm}} = Gm_cm_i\left(\frac{1}{|\mathbf{r}_i|} - \frac{1}{|\mathbf{r}_i-\mathbf{r}_c|}\right),$$

the particle perturbation Hamiltonian caused by the motion of the central body.

We want to know how the magnitude of this extra perturbation term $(\mathcal{H}_i)_{\text{cbm}}$ relates to the Kepler Hamiltonian to determine whether it is small compared to the total Hamiltonian $\mathcal{H}$. For $r \gg r_c$, we see that

$$\begin{aligned}\frac{1}{|\mathbf{r}|} - \frac{1}{|\mathbf{r}-\mathbf{r}_c|} &= \frac{1}{r} - \frac{1}{r\sqrt{1+\left(\frac{r_c^2}{r^2} - \frac{2\mathbf{r}\cdot\mathbf{r}_c}{r^2}\right)}} \\ &= \frac{1}{r} - \frac{1}{r}\left[1 - \frac{1}{2}\left(\frac{r_c^2}{r^2} - \frac{2\mathbf{r}\cdot\mathbf{r}_c}{r^2}\right) + \frac{3}{8}\left(\frac{r_c^2}{r^2} - \frac{2\mathbf{r}\cdot\mathbf{r}_c}{r^2}\right)^2 + \ldots\right] \\ &= \frac{r_c^2}{2r^3} - \frac{\mathbf{r}\cdot\mathbf{r}_c}{r^3} - \frac{3}{8r}\left(\frac{r_c^2}{r^2} - \frac{2\mathbf{r}\cdot\mathbf{r}_c}{r^2}\right)^2 + \ldots,\end{aligned}$$

from which it follows that

$$\left|\frac{1}{|\mathbf{r}|} - \frac{1}{|\mathbf{r}-\mathbf{r}_c|}\right| = \frac{r_c}{r^2} + \mathcal{O}\left(\frac{r_c^2}{r^3}\right). \quad (2.40)$$

Using Equation (2.32) for the total energy of a body in a Kepler orbit, we compute the ratio

$$\left|\frac{(\mathcal{H}_i)_{\text{cbm}}}{(\mathcal{H}_i)_{\text{Kep}}}\right| = \left|\frac{Gm_cm_i}{|\mathbf{r}_i|} - \frac{Gm_cm_i}{|\mathbf{r}_i - \mathbf{r}_c|}\right| \frac{2a_i}{Gm_cm_i} \approx \frac{2a_ir_c}{r_i^2} \approx \frac{2r_c}{r_i} \ll 1. \tag{2.41}$$

Hence, the perturbation caused by the motion of the central body is small compared to the Kepler Hamiltonian and thus also the total Hamiltonian. For instance, in the case of Mercury, the planet closest to the Sun, we have that $2r_{\text{Sun}}/r_{\text{Mercury}} \approx 3 \cdot 10^{-2}$. Although this value is small, it can still cause undesirable numerical errors. Using another coordinate system, such as Jacobian coordinates (see Sec. 1), might be more suitable in this case.

We can do a similar calculation to get the relative size of the two types of perturbations on body i, that is, the ratio of the perturbation caused by the motion of the central body to the perturbation caused by the gravitational interaction between other bodies. We then get that

$$\begin{aligned}\left|\frac{(\mathcal{H}_i)_{\text{cbm}}}{(\mathcal{H}_i)_{\text{int}}}\right| &= \left|\frac{Gm_cm_i}{|\mathbf{r}_i|} - \frac{Gm_cm_i}{|\mathbf{r}_i - \mathbf{r}_c|}\right| \frac{1}{N-1}\left(\frac{\overline{r}_{iN}}{Gm_i\overline{m}_{iN}}\right) \\ &\approx \frac{1}{N-1}\frac{m_c}{\overline{m}_{iN}}\left(\frac{r_c\overline{r}_{iN}}{r_i^2}\right),\end{aligned} \tag{2.42}$$

or, since[4] we have that $\overline{r}_{iN} = \mathcal{O}(r_i)$, we can write

$$\left|\frac{(\mathcal{H}_i)_{\text{cbm}}}{(\mathcal{H}_i)_{\text{int}}}\right| = \mathcal{O}\left(\frac{1}{N-1}\frac{m_c}{\overline{m}_{iN}}\frac{r_c}{r_i}\right).$$

As before, $\overline{m}_{iN}$ denotes the average mass of bodies $j \neq i$ and $\overline{r}_{iN}$ denotes the average distance from body i to bodies $j \neq i$. Unfortunately, we cannot say which perturbation term is larger in general. If one desires more insight into the relative size of the terms, the ratio has to be studied on a case-by-case basis.

For example, consider a selection of bodies from the Solar System. Assume that the Sun and the planets Mercury, Earth, Jupiter and Neptune (and the origin) are on one line (so their relative distances are just differences of their radial distances). The ratio in Equation (2.42) is calculated with $N = 2$ for some combinations of bodies i and j in Table 3. The table shows that in this case, the central body motion perturbation dominates for small r_i. According to Equation (2.42), the perturbation caused by the gravitational pull of other bodies should dominate in the limit $r_i \to \infty$, which is in agreement with the values in Table 3.

From Equation (2.38) is follows that, for $i = 1 \dots N$,

$$(\dot{\mathbf{v}}_i)_{\text{pert}} = Gm_c\left(\frac{\mathbf{r}_i}{|\mathbf{r}_i|^3} - \frac{\mathbf{r}_i - \mathbf{r}_c}{|\mathbf{r}_i - \mathbf{r}_c|^3}\right) - \sum_{j\neq i}\frac{Gm_j}{|\mathbf{r}_i - \mathbf{r}_j|^3}(\mathbf{r}_i - \mathbf{r}_j). \tag{2.43}$$

The value for $\mathbf{r}_c$ is still unknown. To find it, we use Hamilton's equations for the central body. This leads to

$$\dot{\mathbf{r}}_c = \frac{\partial \mathcal{H}}{\partial \mathbf{p}_c} = \frac{\mathbf{p}_c}{m_c} = \mathbf{v}_c,$$

[4]Observe that $\overline{r}_{iN} = \frac{1}{N-1}\sum_{j\neq i}^{N}|\mathbf{r}_i - \mathbf{r}_j| \leq r_i + \frac{1}{N-1}\sum_{j\neq i}^{N} r_j \leq r_i + \max_{j\neq i} r_j$ and thus, as $\max_{j\neq i} r_j$ is a constant a for fixed time t, we have $\overline{r}_{iN} = \mathcal{O}(r_i)$.

Table 3: Ratio given in Equation (2.42) with $N = 2$ for pairs i, j, with $m_c = m_{\text{Sun}}$. Since $N = 2$, we have $\overline{m}_{iN} = \overline{m}_{i2} = m_j$ and $\overline{r}_{iN} = \overline{r}_{i2} = |r_i - r_j|$. The values from Table 2 are used for the calculations, and we assume that all the bodies and the origin are on one line.

Body i	Body j	Ratio
Mercury	Jupiter	$1 \cdot 10^2$
Earth	Jupiter	$2 \cdot 10^1$
Neptune	Jupiter	$1 \cdot 10^{-1}$
Mercury	Earth	$6 \cdot 10^3$
Jupiter	Earth	$3 \cdot 10^2$
Neptune	Earth	$5 \cdot 10^1$

where $\mathbf{v}_c$ is the velocity of the central body, and

$$\dot{\mathbf{p}}_c = -\frac{\partial \mathcal{H}}{\partial \mathbf{r}_c} = -\sum_{i=1}^{N} \frac{G m_c m_i}{|\mathbf{r}_i - \mathbf{r}_c|^3}(\mathbf{r}_i - \mathbf{r}_c).$$

We can now use numerical integration to obtain the central body's position after a time step $\Delta t = t^1 - t^0$, with

$$\mathbf{r}_c(t^1) \approx \mathbf{r}_c(t^0) + \mathbf{v}_c(t^0)\Delta t.$$

Its velocity is obtained with

$$\mathbf{v}_c(t^1) \approx \mathbf{v}_c(t^0) - \sum_{i=1}^{N} \frac{G m_i}{|\mathbf{r}_i(t^1) - \mathbf{r}_c(t^1)|^3}(\mathbf{r}_i(t^1) - \mathbf{r}_c(t^1))\Delta t,$$

and use these values in Equation (2.43) to obtain $(\dot{\mathbf{v}}_i)_{\text{pert}}$.

There is, however, an easier (and perhaps more precise) method to keep track of the central body position and velocity. Define the centre of mass of the system with total mass m_{tot} by

$$\mathbf{r}_{\text{cm}} = \frac{1}{m_{\text{tot}}}\left(m_c \mathbf{r}_c + \sum_{j=1}^{N} m_j \mathbf{r}_j\right). \tag{2.44}$$

By conservation of momentum, we see, after differentiating Equation (2.44), that the centre of mass has a constant velocity, so we can choose an inertial frame of reference such that $\dot{\mathbf{r}}_{\text{cm}} = \mathbf{0}$. By setting $\mathbf{r}_{\text{cm}} = \mathbf{0}$, it follows that

$$\mathbf{r}_c = -\frac{1}{m_c}\sum_{i=1}^{N} m_j \mathbf{r}_i = -\sum_{i=1}^{N} \mu_i \mathbf{r}_i, \tag{2.45}$$

where $\mu_i := m_i/m_c$. By differentiating the central body's position, we also have

$$\mathbf{v}_c = -\sum_{i=1}^{N} \mu_i \mathbf{v}_i. \tag{2.46}$$

We can now use Equation (2.43) together with Equation (2.45) to calculate $(\dot{\mathbf{v}}_i)_{\text{pert}}$ and approximate the position of the body with Equation (2.28).

2.4.4 Special case: the two-body problem

The simplest system to consider is the one with $N = 1$, i.e. the two-body problem with $m_1 = m \ll m_c$. In this case, Equation (2.43) reduces to

$$(\dot{\mathbf{v}}_{\text{pert}})_{N=1} = Gm_c \left(\frac{\mathbf{r}}{|\mathbf{r}|^3} - \frac{\mathbf{r} - \mathbf{r}_c}{|\mathbf{r} - \mathbf{r}_c|^3} \right), \tag{2.47}$$

with $\mathbf{r}$ the position of the orbiting body. According to Equation (2.45), $\mathbf{r}_c = -(m/m_c)\mathbf{r} = -\mu\mathbf{r}$, where $\mu = m/m_c \ll 1$. Hence, the above becomes

$$\begin{aligned}
(\dot{\mathbf{v}}_{\text{pert}})_{N=1} &= Gm_c \left(\frac{\mathbf{r}}{|\mathbf{r}|^3} - \frac{\mathbf{r} + \mu\mathbf{r}}{|\mathbf{r} + \mu\mathbf{r}|^3} \right) \\
&= \frac{Gm_c}{r^2} \left[1 - \frac{1}{(1+\mu)^2} \right] \hat{\mathbf{r}} \\
&= \frac{Gm_c}{r^2} \left[1 - (1 - 2\mu + 3\mu^2 + \dots) \right] \hat{\mathbf{r}} \\
&\approx \frac{2\mu G m_c}{r^2} \hat{\mathbf{r}} = \frac{2Gm}{r^2} \hat{\mathbf{r}}.
\end{aligned}$$

For this scenario, the perturbation $\mathcal{H}_{\text{cbm}}$ results in an acceleration in the direction of $\mathbf{r}$, which causes the body's orbit to change. This effect is substantial, especially for more massive particles, as $(\dot{\mathbf{v}}_{\text{pert}})_{N=1}$ is proportional to m. This means that the perturbed solution, given by Equations (2.28) and (2.47), does not agree with the unperturbed solution of the two-body problem, for which the orbits do not change over time. We would thus prefer to have $(\dot{\mathbf{v}}_{\text{pert}})_{N=1} = \mathbf{0}$. Hence, we write the Hamiltonian in Equation (2.37) as

$$\begin{aligned}
\mathcal{H}^*(\mathbf{z}_1, \dots, \mathbf{z}_N, \mathbf{z}_c) = \frac{p_c^2}{2m_c} &+ \sum_{i=1}^{N} \left(\frac{p_i^2}{2m_i} - \frac{1}{(1+\mu_i)^2} \frac{Gm_c m_i}{|\mathbf{r}_i|} \right) \\
&+ \sum_{i=1}^{N} \left(\frac{1}{(1+\mu_i)^2} \frac{Gm_c m_i}{|\mathbf{r}_i|} - \frac{Gm_c m_i}{|\mathbf{r}_i - \mathbf{r}_c|} \right) - \sum_{i=1}^{N} \sum_{j=i+1}^{N} \frac{Gm_i m_j}{|\mathbf{r}_i - \mathbf{r}_j|} \\
= \frac{p_c^2}{2m_c} &+ \sum_{i=1}^{N} \left(\frac{p_i^2}{2m_i} - \frac{Gm_{ci}^* m_i}{|\mathbf{r}_i|} \right) \\
&+ \sum_{i=1}^{N} \left(\frac{Gm_{ci}^* m_i}{|\mathbf{r}_i|} - \frac{Gm_c m_i}{|\mathbf{r}_i - \mathbf{r}_c|} \right) - \sum_{i=1}^{N} \sum_{j=i+1}^{N} \frac{Gm_i m_j}{|\mathbf{r}_i - \mathbf{r}_j|},
\end{aligned} \tag{2.48}$$

where we have defined the *effective* central mass $m_{ci}^* := m_c/(1+\mu_i)^2$. Note that this does not change the Hamiltonian, as the terms with m_{ci}^* cancel out. With this modification, the two-body problem Hamiltonian is now given by

$$\mathcal{H}^*(\mathbf{z}, \mathbf{z}_c)_{N=1} = \frac{p_c^2}{2m_c} + \left(\frac{p^2}{2m} - \frac{Gm_c^* m}{|\mathbf{r}|} \right) + \left(\frac{Gm_c^* m}{|\mathbf{r}|} - \frac{Gm_c m}{|\mathbf{r} - \mathbf{r}_c|} \right)$$

with $m_c^* = m_c/(1+\mu)^2$. In this case, we get that (see Eq. (2.47))

$$(\dot{\mathbf{v}}^*_{\text{pert}})_{N=1} = \frac{Gm_c^*}{|\mathbf{r}|^3}\mathbf{r} - \frac{Gm_c}{|\mathbf{r}-\mathbf{r}_c|^3}(\mathbf{r}-\mathbf{r}_c)$$

$$= Gm_c\left[\frac{1}{(1+\mu)^2}\frac{\mathbf{r}}{|\mathbf{r}|^3} - \frac{\mathbf{r}+\mu\mathbf{r}}{|\mathbf{r}+\mu\mathbf{r}|^3}\right] = \mathbf{0}.$$

We conclude that the Hamiltonian $\mathcal{H}^*$ introduced here models the two-body problem more accurately than the Hamiltonian $\mathcal{H}$ from Equation (2.37). For the general case with $N > 1$ orbiting particles,

$$(\dot{\mathbf{v}}^*_i)_{\text{pert}} = \left(\frac{Gm_{ci}^*}{|\mathbf{r}_i|^3}\mathbf{r}_i - \frac{Gm_c}{|\mathbf{r}_i-\mathbf{r}_c|^3}(\mathbf{r}_i-\mathbf{r}_c)\right) - \sum_{j\neq i}\frac{Gm_j}{|\mathbf{r}_i-\mathbf{r}_j|^3}(\mathbf{r}_i-\mathbf{r}_j). \tag{2.49}$$

With the effective central mass, the Kepler Hamiltonian for each particle i is given by

$$(\mathcal{H}^*_i)_{\text{Kep}} = \frac{p_i^2}{2m_i} - \frac{Gm_{ci}^* m_i}{|\mathbf{r}_i|},$$

which is the Hamiltonian for a particle orbiting a body situated at the origin with mass m_{ci}^* instead of m_c. This means that the central mass m_c should be replaced by the effective central mass m_{ci}^* in the equations that are used for transforming between the Kepler and Cartesian coordinates (Sec. 2.2), and in the equations used for advancing a body along its orbit (Sec. 2.3).

2.5 The Simulation

We simulate a system of N particles with masses m_i orbiting a central body with mass $m_c \gg m_i$ for all $i = 1, \ldots, N$, and assume that there are no collisions between these particles. Each non-central particle is initialised with the orbital elements

$$(a_i^0, \quad \epsilon_i^0, \quad M_i^0, \quad I_i^0, \quad \Omega_i^0, \quad \varpi_i^0) \tag{2.50}$$

as given in (2.11), with the phase offset ϕ replaced by the mean anomaly M. By Equation (2.6), the States (2.50) and (2.11) are equivalent. The initial value of the eccentric anomaly E_i^0 is calculated using Kepler's equation. The initial position and velocity vectors $\mathbf{r}_i^0$ and $\mathbf{v}_i^0$ are calculated using methods described in Section 2.2.2. At the start of each iteration k of the simulation, we assume that the time-dependent variables

$$\{\mathbf{r}_i^k, \quad \mathbf{v}_i^k\} \tag{2.51}$$

are known. We run the simulation for K iterations. The time at iteration k is denoted by t^k, and so the initial time is t^0. We use a fixed time step Δt, so the total simulated time $t_{\text{sim}} = t^K - t^0 = K\Delta t$. Recall that we have two methods to advance a body along its orbit. Method A utilises the rotation matrix, while Method B makes use of the f and g functions (see Sec. 2.3). For both methods, we discuss how to integrate them into the simulation. The main loop of the simulation is as follows:

1. From $\mathbf{r}_i^k$ and $\mathbf{v}_i^k$, compute the variables needed for this iteration. The specific variables needed differ for the two methods. If $k = 0$, this step can be skipped; go to Step 2.

Method A: calculate the values given in (2.50), excluding the mean anomaly, using the method described in Section 2.2.1. Calculate E_i^k using Equation (2.5).

Method B: only ϵ_i^k and a_i^k are needed. Calculate their values using Equations (2.15) and (2.16). It is, however, convenient to now also calculate the variables that are needed for the analysis of the simulation, but those can also be calculated after the simulation is finished to reduce the runtime.

For both methods, also calculate the mean motion ω_i^k.

2. Advance each particle i along its orbit over a time step Δt. Variables labelled with a prime are intermediate values where the perturbation has not yet been accounted for.

   Method A: use Equation (2.8) to get the eccentric anomaly $(E_i^{k+1})'$ from E_i^k. Use Equations (2.20) and (2.22) with $(E_i^{k+1})'$ in order to obtain $\left(\mathbf{r}_i^{k+1}\right)'$ and $\left(\mathbf{v}_i^{k+1}\right)'$.

   Method B: obtain ΔE^k by employing Equation (2.9). Directly compute $\left(\mathbf{r}_i^{k+1}\right)'$ and $\left(\mathbf{v}_i^{k+1}\right)'$ from $\mathbf{r}_i^k$ and $\mathbf{v}_i^k$ using Equations (2.23) and (2.24).

3. Calculate the change in velocity $\dot{\mathbf{v}}_i^k$ caused by the perturbations using $\left(\mathbf{r}_i^{k+1}\right)'$ and $\left(\mathbf{v}_i^{k+1}\right)'$ in Equation (2.43) or (2.49). Note that when using the latter, m_c needs to be replaced by m_{ci}^* in most equations (see Sec. 2.4.4). If the central body is assumed to be fixed at the origin, use Equation (2.34) instead. Next, set

   $$\mathbf{r}_i^{k+1} = \left(\mathbf{r}_i^{k+1}\right)'$$

   and compute

   $$\mathbf{v}_i^{k+1} = \left(\mathbf{v}_i^{k+1}\right)' + (\dot{\mathbf{v}}_i^k)_{\text{pert}} \Delta t.$$

4. Update the time $t^{k+1} = t^k + \Delta t$ and iteration $k \to k+1$.

5. If $k = K$ or $\epsilon_i^k \geq 1$ for some particle i, end the simulation. Otherwise, go back to Step 1.

Note that in Step 5, we end the simulation if at least one particle's orbit changed from bounded to unbounded ($\epsilon \geq 1$). The issue with an unbounded particle is that it still contributes to the position of the centre of mass and thus the position of the central body (Equations (2.44) and (2.45)). One could also delete particle i from the simulation whenever $\epsilon_i^k \geq 1$ and adjust the centre of mass accordingly (note that there is a possibility that the particle could end up in a bounded orbit again). Alternatively, one could simulate the particle's orbit as a parabola or a hyperbola in the case that it becomes unbounded.

The simulation method does not currently support orbits with $\epsilon = 0$, since it requires the argument of periapsis to be defined (see Eq. 2.18), at least when initialising the particles. For Method A, the eccentricity has to be non-zero for advancing a body along its orbit as well. Although Method B does not rely on the eccentricity being non-zero to do this, a non-zero eccentricity is still necessary to calculate the orbital elements in (2.11) that may be needed for analysis. Alternatively, a circular orbit can be modelled as an elliptical orbit with a sufficiently small value for the eccentricity.

In Step 3 we calculate $(\dot{\mathbf{v}}_i^k)_{\text{pert}}$ using the value of $\left(\mathbf{z}_i^{k+1}\right)'$ in Equation (2.43). One could also use the value of $\mathbf{z}_i^k$ or a weighted sum of the two different values for this calculation. In this last case, we get an integration method similar to Leapfrog integration (Murray & Dermott 2009), which might result in smaller numerical errors. However, such methods are not used here since we include simulations where $\Delta t > T_i$ for some body i.

The simulation method is implemented in Python. The source code can be found on GitHub (van der Ven 2025).

3 Results and discussion

In this section, we analyse the simulation method outlined in Section 2.5. We first investigate the difference between Method A and Method B, and identify the most favourable of the two (Sec. 3.1). Next, we study the dependence of the error on the time step size (Sec. 3.2). We then consider the magnitudes of the perturbation Hamiltonians to determine whether the perturbation is significantly small, and to determine whether the magnitudes agree with the estimates from Sections 2.4.2 and 2.4.3 (Sec. 3.3). Lastly, we use conservation of energy and resonance as a gauge for simulation fidelity (Sec. 3.3 and Sec. 3.4, respectively). For all dynamic Sun simulations discussed, we make use of the effective central mass m^*_{ci}, introduced in Section 2.4.4.

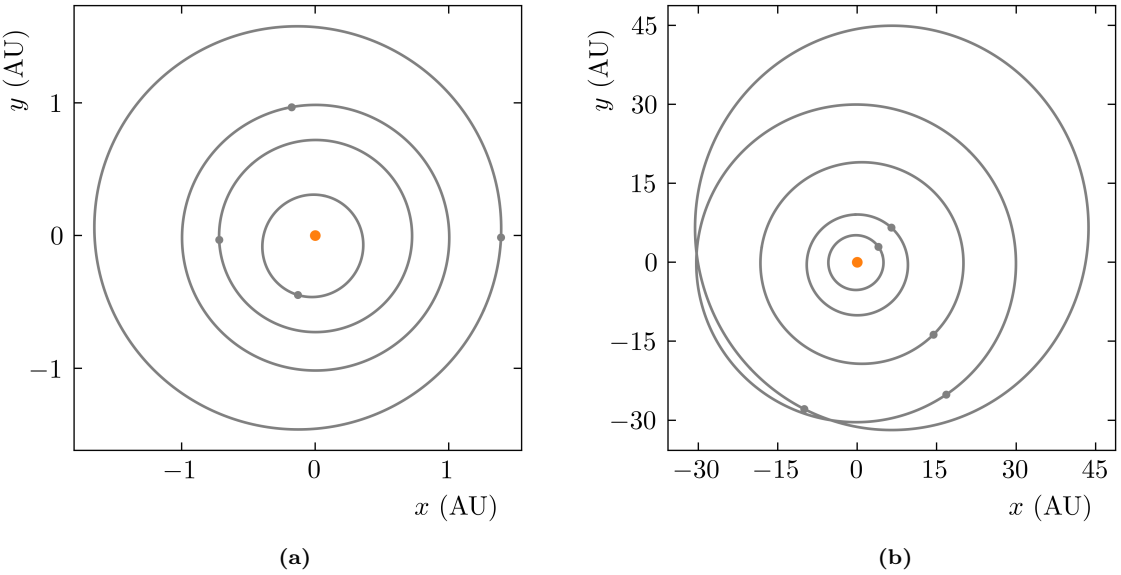

Figure 5: Projection of orbits in the Solar System onto the xy-plane for, in order of increasing a, the planets (a) Mercury, Venus, Earth, and Mars, and (b) Jupiter, Saturn, Uranus, Neptune, and Pluto (see also Fig. 2). These are the orbits on the 1st of January, 2000, and the positions of the planets on that date are indicated with a dot. The Sun, situated at the origin, is shown in orange.

We analyse the simulation's performance for the Solar System and the restricted three-body problem. For our purposes, the Solar System contains the nine planets Mercury, Venus, Earth, Mars, Jupiter, Saturn, Uranus, Neptune, and Pluto, with the Sun as its central body. Figure 5 shows the projection of the orbits for these planets onto the xy-plane on the 1st of January, 2000. The Sun's position is shown in orange, and the planets' position is shown by a dot on the orbit. This configuration is the start position for the analysed simulations of the Solar System. Note the large eccentricity of Pluto's orbit. The data for this system are obtained from both Murray & Dermott (2009) and Williams (2016). Figures 6(a) and 6(b) show the simulated change in the orbits from Figure 5 after, respectively, $6 \cdot 10^4$ years and 10^5 years. Note the big shift in Mars's periapsis.

The system for analysis of the restricted three-body problem consists of Jupiter orbiting the Sun in a circular orbit ($\epsilon_{\text{Jupiter}} \ll 1$), and a test particle, which experiences the gravitational pull from the other bodies, but does not itself exert a gravitational force on the other bodies.

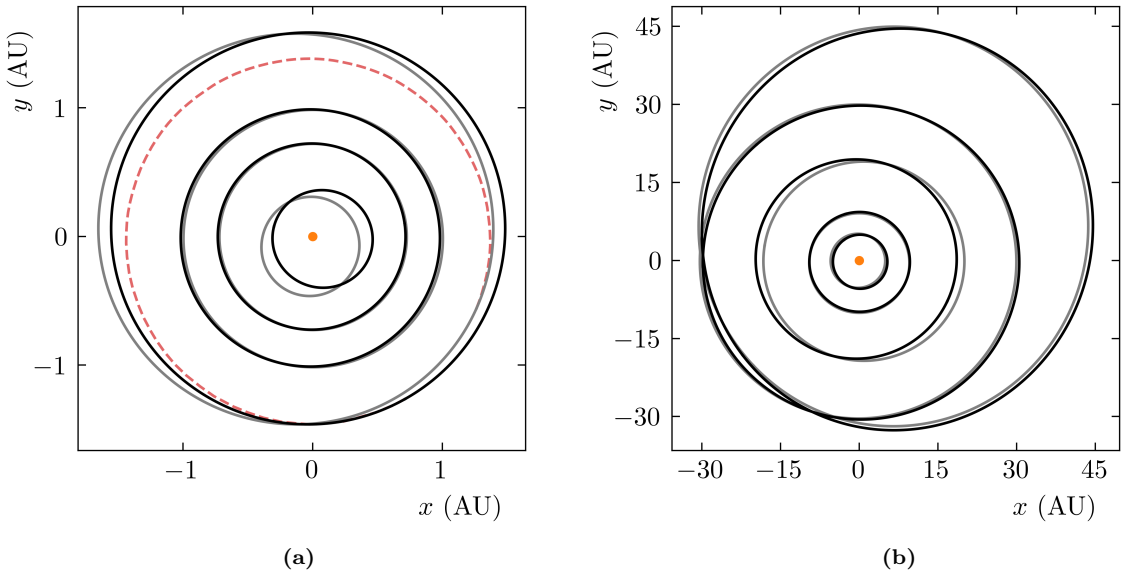

(a) **(b)**

Figure 6: Projection of orbits in the Solar System onto the xy-plane on the 1st of January, 2000 (grey), and their simulated ($\Delta t = 0.8$ y, Sun fixed at the origin, Method B) orbits after (a) $6 \cdot 10^4$ y and (b) 10^5 y (black) for the same planets as in Figures 5(a) and 5(b), respectively. Mars has the largest periapsis precession, and the trajectory of its periapsis is shown by the red dashed curve.

3.1 Method A versus Method B

In Section 2.3, we discussed two potential advantages of using Method B over Method A. The runtime of simulations using Method B may be shorter, as Method B requires fewer calculations than Method A. Furthermore, simulations using Method B may have smaller numerical errors, especially for small eccentricity ϵ, since in that case the eccentric anomaly E is ill-defined, while the change in eccentric anomaly ΔE is not.

Figure 7 shows the runtimes for simulations using Method A and Method B, labelled 'A' and 'B', respectively. Simulations using Method B are 30-40% faster than simulations using Method A. Recall from Section 2.5, however, that when storing particle data at every iteration, extra calculations need to be done for Method B. Simulations that store data are labelled 'A/store' and 'B/store'. For Method A, the runtime does not increase significantly, but for Method B, the runtime is now similar to the runtime of Method A. Method B is thus favoured when data at only a selected number of iterations need to be stored.

Since E is ill-defined for small values of ϵ, one may expect the error $|\epsilon^K - \epsilon^0|$ between the initial eccentricity ϵ^0 and the eccentricity ϵ^K after K iterations to be greater for small values of ϵ^0 when using Method A. This relation is depicted in Figure 8, which shows the error $|\epsilon^K - \epsilon^0|$ for both methods as a function of ϵ^0 for the planets Mercury, Mars, Jupiter, and Neptune in the two-body system with the Sun and the planets. Contrary to expectations, the magnitude of the error does not differ significantly between the methods. Interestingly, for unknown reasons, Mercury's and Mars's error (Figs. 8(a) and 8(b)) for Method B is significantly greater than the error for Method A, when ϵ^0 is in the interval $(10^{-2}, 1)$. This is also the case for Venus and Earth (not shown in Fig. 8). This might be caused by the difficulty of numerically solving for ΔE in Equation (2.9), especially for larger eccentricities, but further analysis is needed to draw any conclusions. Nonetheless, the error remains below 10^{-10}, which is negligibly small compared to the global error due to numerical integration (see Sec. 3.2). Observe that for both methods, even though the *absolute* error remains small for all initial values ϵ^0, the *relative* error $|\epsilon^K - \epsilon^0|/\epsilon^0$ exceeds unity for small values of ϵ^0. One should thus be cautious when simulating particles with eccentricities $< 10^{-10}$. However, such small eccentricity values are several orders of magnitude smaller than the measurement error. Only when modelling a circular orbit as an elliptical orbit with small eccentricity, eccentricities of this order might be considered. However, a value of $\epsilon \approx 10^{-5}$ should suffice in this case.

As Method A and Method B produce very similar results, we mostly use Method B in the sections below due to its shorter runtime, and omit the specification of which method is used.

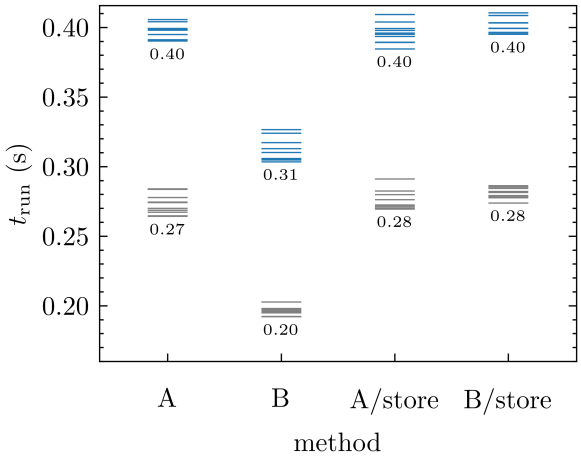

Figure 7: Runtimes t_{run} for ten repetitions of eight different simulations of the Solar System with $K = 1000$ iterations ($t_{\mathrm{sim}} = 10$ y, $\Delta t = 0.01$ y), using Method A, using Method B, and using Method A or B and storing the orbital elements for all bodies at every iteration, labelled 'A/store' and 'B/store', respectively. Runtimes of simulations without any perturbation are shown in grey, and with interaction and central body motion perturbations are shown in blue. The mean of the runtimes is shown below the corresponding data points.

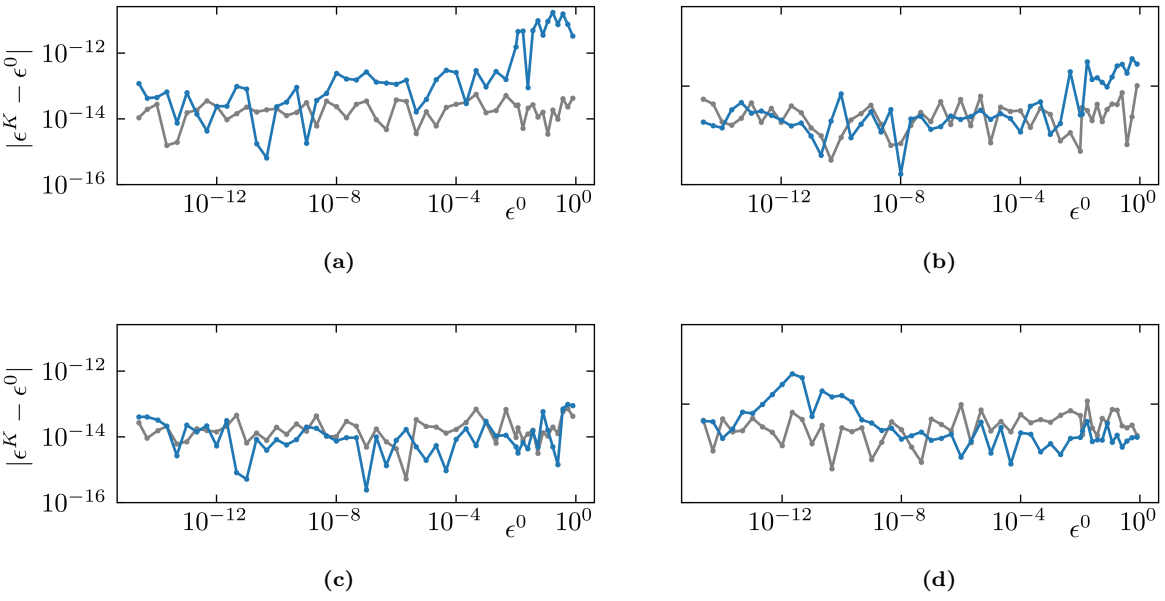

Figure 8: Error $|\epsilon^K - \epsilon^0|$ between initial eccentricity ϵ^0 and final eccentricity ϵ^K of the planets (a) Mercury, (b) Mars, (c) Jupiter, and (d) Neptune as function of the start value ϵ^0 for the two-body (Sun and planet) simulations ($K = 10^5$, $t_{\mathrm{sim}} = 10^4$ y, $\Delta t = 0.1$ y, Sun fixed) using Method A (grey) and Method B (blue). Observe that for Mercury and Mars, when $\epsilon^0 > 10^{-2}$, the error for Method B is significantly larger than for Method A. Nevertheless, this error remains below 10^{-10}.

3.2 Error analysis

In this section, we investigate the error of simulations of the Solar System. Specifically, we consider the *global relative* error, which is the relative error after multiple time steps (contrary to the *local* error, which is the error after one time step), defined as $\eta_\epsilon = |\epsilon - \epsilon_{\text{ref}}|/\epsilon_{\text{ref}}$. Here, ϵ is a planet's eccentricity at $t = t_{\text{sim}}$ obtained from a simulation with time step Δt, and ϵ_{ref} is the reference eccentricity, also at $t = t_{\text{sim}}$, obtained from a simulation with $\Delta t_{\text{ref}} \ll \Delta t$. We examine simulations with different time steps Δt, but equal simulated time t_{sim}. When $\Delta t = nT_i$, with n a positive integer, time step resonance can occur. In this case, body i is in the same position when calculating the perturbation every iteration, leading to a less accurate model[5]. Hence, we consider the case with $\Delta t < T_i$ and the case without restrictions on Δt separately.

Figure 9 shows the relative error η_ϵ for simulations of the Solar System for the planets Mercury, Mars, Jupiter, and Neptune ($t_{\text{sim}} = 5$ y). Simulations with the Sun fixed are shown in black, and simulations with a dynamic Sun are shown in blue. For simulations with a dynamic Sun, the time step is limited to $\Delta t < T_{\text{Mercury}}$. Otherwise, Mercury ends up in an unbounded orbit due to large errors, and the simulation is terminated pre-emptively. Linear fits of the logarithmic values of the data points show that $\eta_\epsilon = \mathcal{O}\left(\Delta t^p\right)$ with $p \approx 1$ for both the fixed and dynamic Sun simulations. We refer to Table 5 in Appendix C for an overview of the detailed fit parameters, including their errors. Only the error for Mercury deviates from this trend, with $p = 1.28$ for the fixed Sun simulations and $p = 0.8$ for the dynamic Sun simulations, the latter suggesting an increased sensitivity to the central body motion perturbation for inner orbits. When the data point at the largest value of Δt ($= 0.15$ y) is excluded from the fit of the dynamic Sun simulations in Figure 10(a), the slope, and hence also p equals 1.03 ± 0.08. This is more in line with the values of p for the other planets. The smaller error for the simulation with $\Delta t = 0.15$ y is possibly a statistical outlier. Without this data point, the largest time step that preserves numerical stability for the dynamic Sun simulation is $\Delta t_{\text{max}} = 0.039$ y. In Section 1, we mentioned the limit on the largest possible time step, presented in Viswanath (2002), which is one-sixth of Mercury's orbital period. For the largest possible time step $\Delta t_{\text{max}} = 0.039$ y found here, we have that $T_{\text{Mercury}}/\Delta t_{\text{max}} = 6.2$, which is in line with the results found by Viswanath.

The values of p found are close to the expected value of $p = 1$. We expect this value because the local truncation error is $\mathcal{O}(\Delta t^2)$, as each integration step is a linearisation, and the global error is thus $\mathcal{O}(\Delta t^1)$ (Süli & Mayers 2003). Furthermore, observe that the error of the dynamic Sun simulations is consistently at least as big as the error of the fixed Sun simulations, and that the difference between the magnitude of these two errors decreases when the distance to the Sun increases. This is consistent with Equation (2.40), which says that $(H_i)_{\text{cbm}} = \mathcal{O}(1/r_i^2)$. Therefore, we expect the error to also decrease with increasing distance from the Sun.

Figure 10 shows the error η_ϵ of the same fixed Sun simulations of Figure 9 (shown in black) as a function of time step Δt, but spanning a longer timespan of $t_{\text{sim}} = 1000$ y and including bigger time steps. This includes time steps that exceed the periods of the planets, shown by the vertical grey line in the figures. Simulations with a dynamic Sun are not included because, as explained above, the larger time step results in unbounded

[5]Note that time step resonance can also occur when n is a fraction. However, the effect is most pronounced when n is an integer. Time step resonance may be mitigated by taking $\Delta t = \gamma_1 T_1 + \cdots + \gamma_N T_N$, with γ_i irrational parameters, but such alternatives are not investigated further here.

orbits. The red line indicates where $\eta_\epsilon = 1$, because the relative error should not exceed unity. Although there are significantly more fluctuations in the error with larger time steps, the linear fit is still relatively accurate, with the relative error of the slope fit parameter staying below 10% (see Table 5). However, the slopes themselves range from 0.86 to 1.05, thus being slightly smaller than expected.

Except for Neptune, and especially for the inner planets, we see that simulations with time step $\Delta t > T_i$ are still relatively accurate, with the relative error of Mercury's eccentricity staying below 10% when $\Delta t \approx 10^2 \cdot T_{\text{Mercury}}$, and analogously when $\Delta t \approx 10 \cdot T_{\text{Mars}}$ for Mars's eccentricity. Furthermore, contrary to the dynamic Sun simulations, unbounded orbits happen only for very large time steps, when the relative error exceeds unity. This behaviour may be the result of a kind of *orbit averaging*. If we take t_0 and t_1 such that $\Delta t = t_1 - t_0 = T$, the integral in Equation (2.27) equals, up to the factor $1/\Delta t$, the orbit average of $J\nabla\mathcal{H}_{\text{pert}} = (-\dot{\mathbf{p}}_{\text{pert}}, \dot{\mathbf{r}}_{\text{pert}})$, taken along the Kepler orbit $\mathbf{r}_{\text{Kep}}(t)$ with $t_0 \leq t < t_1$. When we take $\Delta t > T$ and approximate the integral as in Equation (2.28), we do not get the same orbit averaging as with the integral. However, since the planets are in a different location on their orbits during each iteration, provided that an appropriate time step is chosen that mitigates time step resonance, we essentially average over the orbits in this case as well (see Sec. 1 for a more comprehensive explanation). Nevertheless, to get a better understanding of this potential orbit averaging, a statistical framework may be required when evaluating the effect of the perturbation, rather than naively using a large time step in Equation (2.27).

Overall, we conclude that for all simulations, with a fixed or dynamic central body, the error can be predicted accurately for small time steps ($\Delta t < T_{\text{Mercury}}$), since $\eta_\epsilon = \mathcal{O}(\Delta t^p)$ with $p \approx 1$. Furthermore, although we still roughly have that $\eta_\epsilon = \mathcal{O}(\Delta t)$ for simulations with a fixed central body and time step $\Delta t > T_i$ for at least one body i, the simulations are significantly less accurate than when $\Delta t < T_i$. Nevertheless, simulations with big time steps are still viable to reduce the runtime of the simulation when only the qualitative behaviour of a Solar System-like system is required.

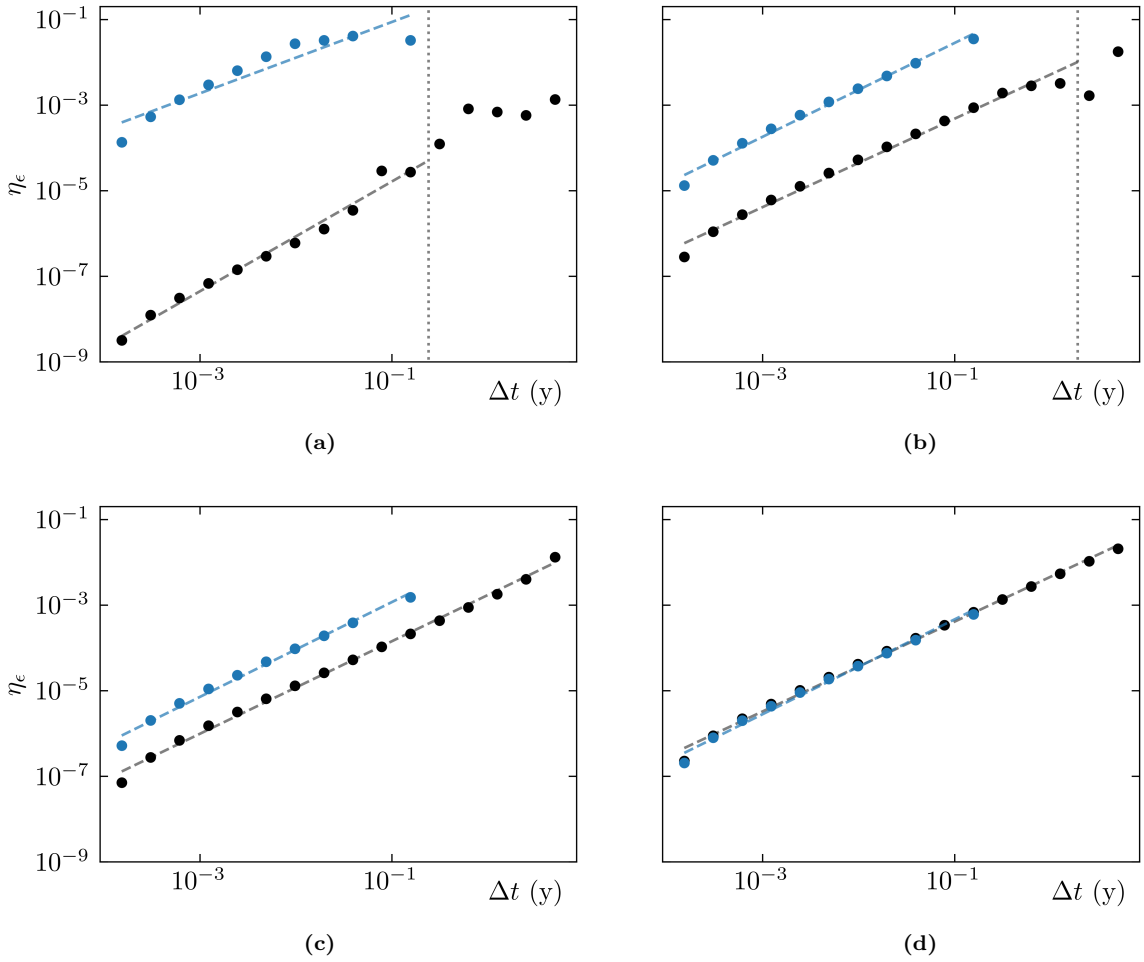

Figure 9: Relative error $\eta_\epsilon = |\epsilon - \epsilon_{\text{ref}}|/\epsilon_{\text{ref}}$ of eccentricities of the planets (a) Mercury, (b) Mars, (c) Jupiter, and (d) Neptune after $t_{\text{sim}} = 5$ y, as function of time step Δt, where ϵ_{ref} is the reference value obtained by simulation with time step $\Delta t_{\text{ref}} = 0.0001$ y, for simulations of the Solar System with the Sun fixed (black), and with a dynamic Sun (blue). The point at which $\Delta t = T$, the planet's orbital period, is indicated with a grey dotted line. Here, an increase in error can be expected due to time step resonance. Numerical fits of the (logarithmic values of the) data points for which $\Delta t < T$ are shown by the dashed lines. The slopes of the fits are (a) 1.28 (black) and 0.8 (blue), (b) 1.03 (black) and 1.10 (blue), (c) 1.08 (black) and 1.11 (blue), and (d) 1.05 (black) and 1.11. The fit parameters with their errors, including the offset not stated here, are given in Table 5 in Appendix C.

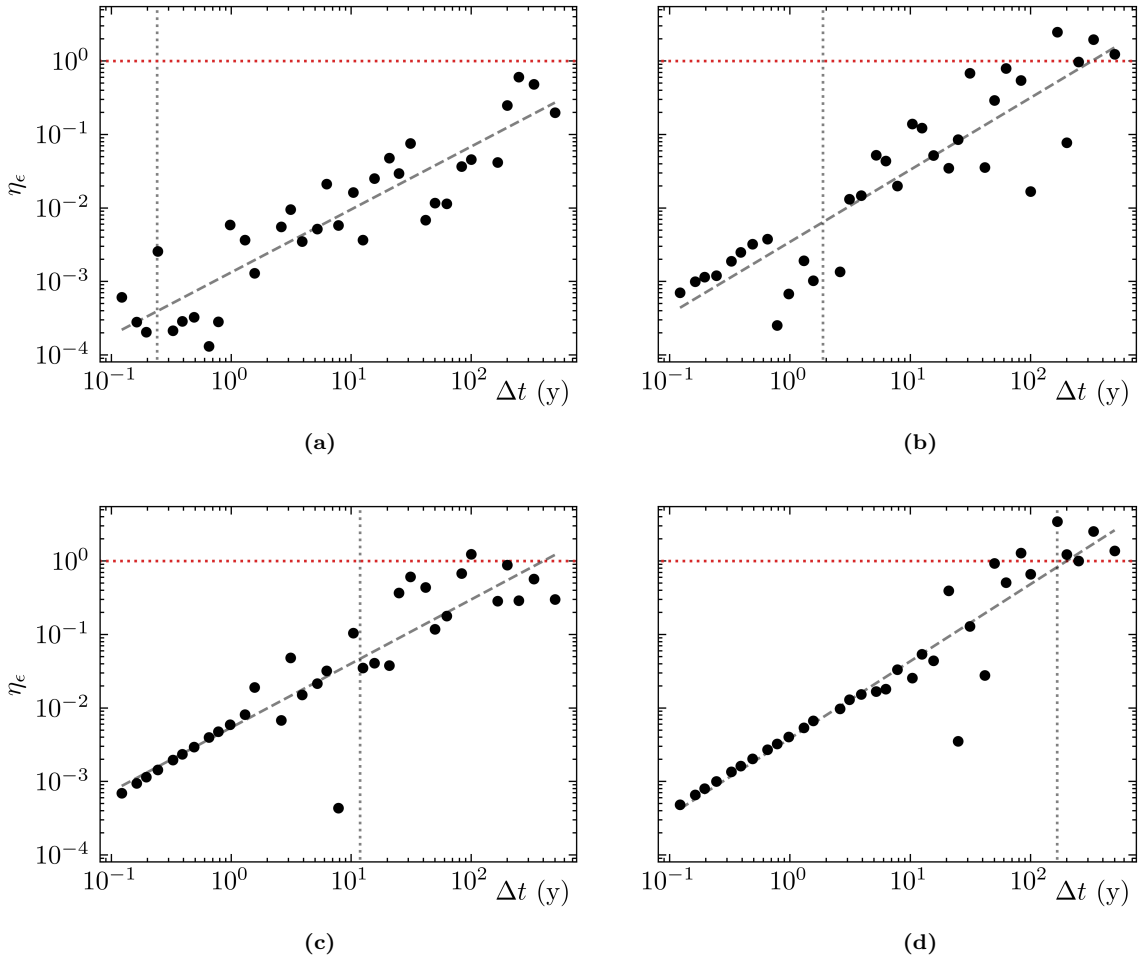

Figure 10: Relative error $\eta_\epsilon = |\epsilon - \epsilon_{\text{ref}}|/\epsilon_{\text{ref}}$ as function of time step Δt as in Figure 9 but with $t_{\text{sim}} = 1000$ y and $\Delta t_{\text{ref}} = 0.01$ y. Only the simulation with fixed Sun is considered. The point at which $\Delta t = T$ is indicated with a grey dotted line. The point at which the relative error $\eta_\epsilon = 1$ is indicated with a red dotted line. Numerical fits of the (logarithmic values of the) data points are shown by the dashed lines. The slopes of the fits are (a) 0.86, (b) 0.98, (c) 0.87, and (d) 1.05. The fit parameters with their errors, including the offset not stated here, are given in Table 5 in Appendix C.

3.3 Perturbation magnitudes and energy conservation

In Sections 2.4.2 and 2.4.3, we estimated $(\mathcal{H}_i)_{\text{int}}$ and $(\mathcal{H}_i)_{\text{cbm}}$ to determine whether the perturbation would remain small compared to the total particle energy. The estimates are given as ratios in Equations (2.33) and (2.41), from which we concluded that for Mercury — or any other body in a small orbit — the dynamic central body perturbation $(\mathcal{H}_i)_{\text{cbm}}$ may be too large. Because of the big discrepancy in the error between the fixed and dynamic Sun simulation in Figure 9, we investigate the magnitude of the perturbation terms further.

Figure 11 shows the relative magnitudes of the different Hamiltonian components as a function of time for the planets labelled above the figures for dynamic Sun simulations of the Solar System. The interaction Hamiltonian $(\mathcal{H}_i)_{\text{int}}$ (shown in blue) remains relatively constant and is at least three orders of magnitude smaller than the Kepler Hamiltonian $(\mathcal{H}_i)_{\text{Kep}}$ (shown in grey). In contrast, the perturbation Hamiltonian $(\mathcal{H}_i)_{\text{cbm}}$ (shown in black) is only two to three orders of magnitude smaller for the inner planets, and larger still for Mercury. Specifically, the ratio $|(\mathcal{H}_{\text{Mercury}})_{\text{cbm}}/(\mathcal{H}_{\text{Mercury}})_{\text{Kep}}|$ has an average value of $1.8 \cdot 10^{-2}$ and a maximum value of $5.7 \cdot 10^{-2}$, which agrees with the estimate found in Section 2.4.3. For simulations with small time step ($\Delta t \ll T_{\text{Mercury}}$), this perturbation is sufficiently small not to cause large errors, but, as is apparent from Figure 9(a), it leads to large errors — or indeed an unbounded orbit — when using bigger time steps ($\Delta t > 10^{-2} \cdot T_{\text{Mercury}}$). For planets in large orbits (Jupiter's orbit and larger), one need not be concerned about this, as $|(\mathcal{H}_{\text{Mercury}})_{\text{cbm}}|$ is roughly equal to or less than $|(\mathcal{H}_{\text{Mercury}})_{\text{int}}|$. Note, however, that the large magnitude of $\mathcal{H}_{\text{cbm}}$ is a problem specific to this system. Due to Jupiter's large mass, r_c is relatively big, and by Equation (2.41), this results in a large relative magnitude of $\mathcal{H}_{\text{cbm}}$. In a system without bodies close to the central body or massive planets in outer orbits, $|(\mathcal{H}_i)_{\text{cbm}}|$ is smaller for all bodies. The simulation may thus be more stable when time steps $\Delta t > T_i$ are used.

As the Solar System is essentially isolated, the total energy should be conserved. The relative total energy deviation of three different simulations of the Solar System is shown in Figure 12(a) as a function of time. The relative total energy deviation of the simulation with fixed Sun and $\Delta t = 0.8$ y (shown in black), and the simulation with dynamic Sun and $\Delta t = 0.01$ y (shown in blue) remains smaller than 10^{-4}. For the simulation with fixed Sun and $\Delta t = 0.01$ (shown in grey), the relative deviation is smaller still, with a maximum value on the order of 10^{-7}. The total energy for these systems thus remains essentially constant. Hence, it is reasonable to expect that they accurately describe the Solar System. It is important to note, however, that energy conservation alone is an insufficient measure when determining the accuracy of a simulation. Other conserved quantities, such as momentum and angular momentum, should be considered as well, since conservation laws for these quantities can also be violated, even when the total energy remains essentially constant. Lastly, note that the fluctuations in the total energy are merely a result of (numerical) error. Ideally, the plots should be a perfect horizontal line.

The effect of the time step size on energy conservation is depicted in Figure 12(b), in which the relative standard deviation $s^K_{E_{\text{tot}}}/|\overline{E}_{\text{tot}}|$ is plotted against time step Δt for fixed Sun simulations with timespan 10^4 y. As expected, because of the larger error, the standard deviation increases as the time step increases. The extent to which the simulation violates energy conservation thus increases with step size. Nevertheless, for simulations with $\Delta t < 10$ y (which is not significantly smaller than T_{Jupiter}), the relative

standard deviation does not exceed 10^{-3}, indicating that the degree to which energy conservation is violated remains minimal. This further suggests that, while simulations with a large time step have relatively large errors, these simulations are valuable to obtain qualitative behaviours of a planetary system.

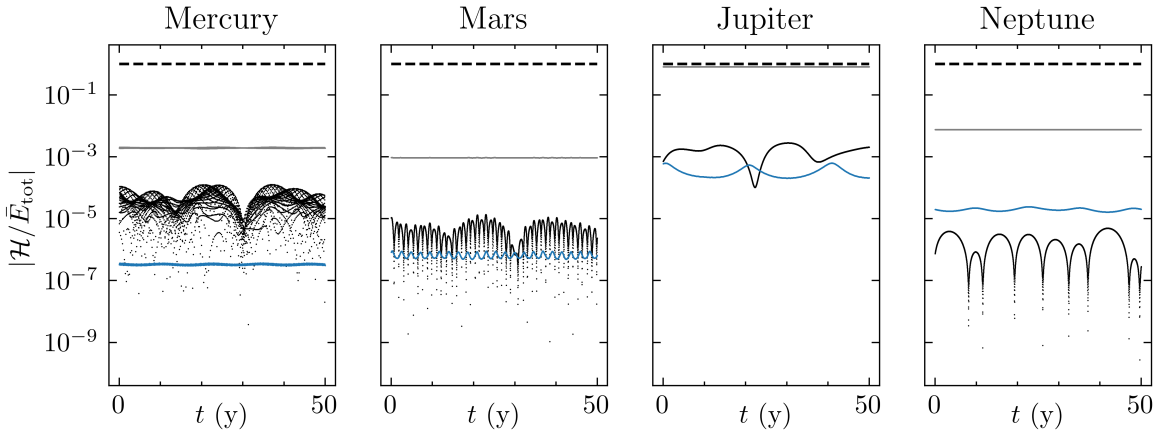

Figure 11: Relative magnitudes $|\mathcal{H}/E_{\text{tot}}|$ of the Hamiltonians $(\mathcal{H}_i)_{\text{Kep}}$ (grey), $(\mathcal{H}_i)_{\text{int}}$ (blue), and $(\mathcal{H}_i)_{\text{cbm}}$ (black) as function of time for the planets in the Solar System indicated above the plots ($\Delta t = 0.01$ y, $t_{\text{sim}} = 50$ y, dynamic Sun). The magnitude of the Hamiltonian of the entire system is depicted by a black dashed line. Observe that for Mercury, the highest values of $(\mathcal{H}_i)_{\text{cbm}}$ are only one to two orders of magnitude smaller than $(\mathcal{H}_i)_{\text{Kep}}$.

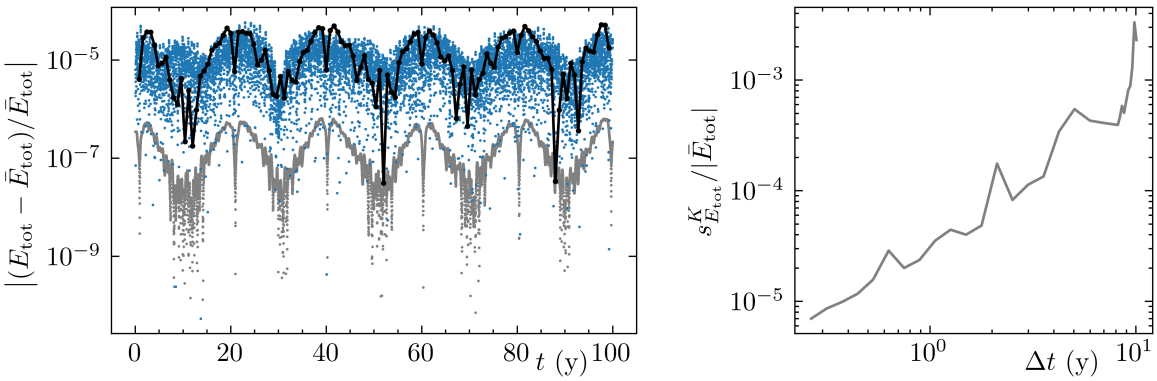

(a) **(b)**

Figure 12: (a) Relative total energy deviation $|(E_{\text{tot}} - \overline{E}_{\text{tot}})/\overline{E}_{\text{tot}}|$ as function of time t for simulations the Solar System with $\Delta t = 0.8$ y and a fixed Sun (black), $\Delta t = 0.01$ y and a fixed Sun (grey), and $\Delta t = 0.01$ y and a dynamic Sun (blue). The data points are represented by dots, and for the simulation with $\Delta t = 0.8$ y, the data points are connected by a line for better readability. (b) Relative (sample) standard deviation $s^K_{E_{\text{tot}}}/|\overline{E}_{\text{tot}}|$ as a function of time step Δt for simulations of the Solar System with the Sun fixed at the origin ($t_{\text{sim}} = 10^4$ y). Note that the number of iterations K, and thus the number of samples for the standard deviation, depends on Δt.

3.4 Resonance as gauge for simulation fidelity

In some cases, high precision of the simulation is essential when investigating the details of the behaviour of a system. The occurrence of resonance in a system is an example of this. We speak of resonance when there is a simple numerical relation between the mean motions of two bodies. Briefly, a resonance between two (or more) planets can occur due to their mutual gravitational attraction keeping them around an equilibrium — when one planet drifts away from this equilibrium, the attraction from the other planet pulls it back to the equilibrium. An example of planets that are in resonance in the Solar System is the pair Neptune and Pluto. They are in a 3:2 resonance, which means that $\omega_{\text{Neptune}}/\omega_{\text{Pluto}} = 3/2$ (Murray & Dermott 2009). To test the accuracy of the simulation with small Δt, and to analyse the effect of the time step size on the accuracy, we consider the restricted three-body problem (see Sec. 3), in which the test particle and Jupiter are in a 2:1 resonance, i.e. $\omega_{\text{test}}/\omega_{\text{Jupiter}} = 2$.

Figure 13 shows the evolution of four quantities important when studying resonance over a timespan of 100 Jupiter periods. Figures (a) – (f) have slightly different initial values for a_{test} and ϵ_{test} (see Table 4). The initial values are chosen such that the test particle and Jupiter are in (the vicinity of) a 2:1 resonance. Each initial condition corresponds to a specific type of resonance, but details of each type are irrelevant for our discussion here[6]. In each figure, the results of four different types of simulations are shown, differing in the position of the Sun (fixed or dynamic) and the initial values (calculated in the centre of mass frame or the heliocentric frame).

From Figure 13, it is immediately apparent that the resulting behaviour of the system is highly sensitive to the initial condition. One can thus imagine that, when the error of the simulation is relatively large, details of the behaviour are lost. Furthermore, the simulation with a fixed Sun and initial values calculated in the heliocentric frame (shown in black), and the simulation with a dynamic Sun and initial values calculated in the centre of mass frame (orange), most accurately reproduce the results given in Murray & Dermott (2009), p. 366, the latter being a remarkable reproduction. In this case, the significance of the effective central mass, introduced in Section 2.4.4, becomes apparent. For the results in the previous sections, exchanging the central mass m_c for the effective central mass m^*_{ci} made little difference. However, possibly due to the sensitivity of the system discussed here, the dynamic Sun simulations give considerably different results (not shown here) when the effective mass is not used, and resonance is not easily found in that case. With a sufficiently small time step, the simulation can thus accurately describe a 2:1 resonance for a restricted three-body problem, especially when the motion of the central body is taken into consideration.

Figure 14 is the same as Figure 13, but the time steps of the simulations are equal to $\Delta t = 2.5$ y < 5.93 y $= T_{\text{test}}$. Comparing the two figures, we see that details of the behaviour are lost when using a bigger time step. This is especially the case for Figures 14(c) – 14(f), in which few similarities with their corresponding figure for $\Delta t = 0.1$ y can be found. Interestingly, the fixed Sun simulation with its initial values calculated in the centre of mass frame (shown in blue) does show some similarities between the two figures. Even though this simulation does not describe the system accurately, the results suggest some degree of stability for larger time steps.

[6] As an example, Figure 13(a) corresponds to *exact* resonance (Murray & Dermott 2009). In this case, we have $T_{\text{Jupiter}} = 2T_{\text{test}}$, and thus $a^0_{\text{hcf}}/a_{\text{Jupiter}} = (1/2)^{2/3} = 0.6299605\ldots$ (see Table 4).

Table 4: Initial values of the test particle's semi-major axis a, eccentricity ϵ and longitude of periapsis Φ, for the simulations of the plots shown in Figures 13 and 14. The values are taken from Murray & Dermott (2009). Here, the values for the semi-major axis a^0_{comf} are calculated in the centre of mass frame. The semi-major axis a^0_{hcf} is the value corresponding to a^0_{comf} adjusted to the heliocentric frame. Note that for Plot (a), a^0_{hcf} is chosen such that $T_{\text{Jupiter}} = 2T_{\text{test}}$, as $a^0_{\text{hcf}}/a_{\text{Jupiter}} = (T^2_{\text{test}}/T^2_{\text{Jupiter}})^{1/3} = (T^2_{\text{test}}/(2T_{\text{test}})^2)^{1/3} = (1/2)^{2/3} \approx 0.6299605$ (see Eq. (2.19)).

Plot	$a^0_{\text{hcf}}/a_{\text{Jupiter}}$	$a^0_{\text{comf}}/a_{\text{Jupiter}}$	ϵ^0	Φ^0 (rad)
(a)	0.629961	0.625277	0.128386	0
(b)	0.638169	0.633424	0.0725011	0
(c)	0.642615	0.637837	0.0122862	0
(d)	0.641475	0.636705	0.060146	π
(e)	0.643003	0.638222	0.0184545	π
(f)	0.615166	0.610592	0.1975	0

Figure 15 shows the relative error η_ϵ as a function of time step Δt for the same simulations as Figures 13 and 14, differing only in time step size. Like Figure 9, it shows that $\eta_\epsilon = \mathcal{O}(\Delta t^p)$, with $p \geq 1$. Contrary to the result in Section 3.2, p exceeds 2 for some simulations of this specific system, which could be due to its simplistic nature: the restricted three-body problem analysed here, versus the Solar System with nine planets analysed in Section 3.2. This difference may also be the result of the fewer data points or the fewer iterations of the simulations used here, compared to the results in Section 3.2. More importantly for the discussion here, we see that for $\Delta t = 2.5$ (indicated by the grey line on the right), we have $10^{-1} \leq \eta_\epsilon \leq 10^0$ for most simulations, with some relative errors exceeding unity (indicated by the red line). These large errors explain the behaviour of Figure 14 discussed above, since the error increases significantly with increasing step size. For $\Delta t = 2.5$ y, the simulations are no longer accurate enough to model the resonance, due to the high sensitivity of this phenomenon. Furthermore, it is clear from Figure 15 that overall, the fixed Sun simulation with its initial values calculated in the centre of mass frame (shown in blue) has the lowest errors, explaining the stability of this specific simulation.

Even though the simulation can accurately describe the details of the system's behaviour, in this case, the phenomenon of resonance, when the motion of the central body is taken into account and the step size is sufficiently small, these details are lost when the time steps become too large. This further substantiates the idea that big time steps are useful mostly when analysing a system qualitatively rather than quantitatively.

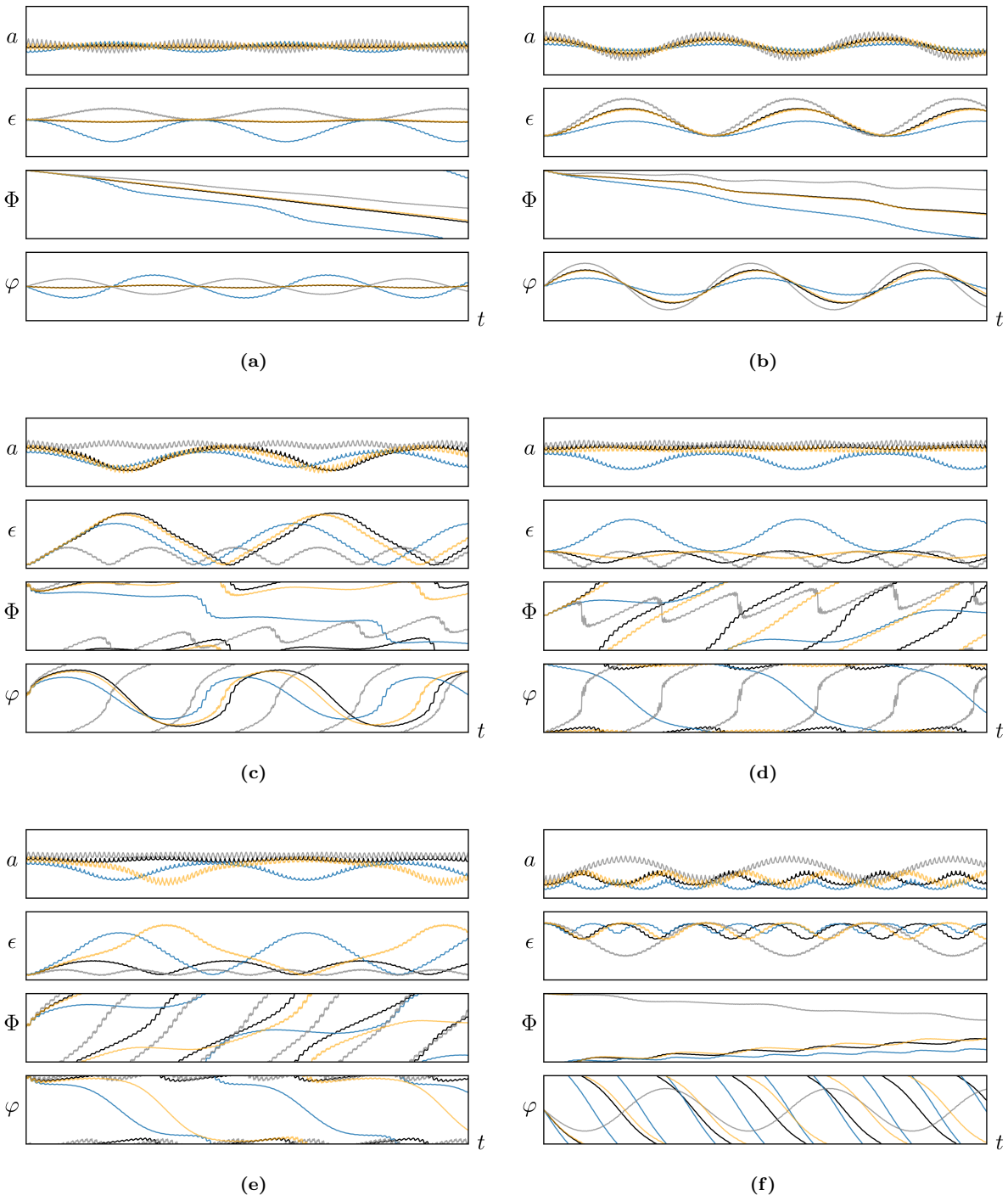

Figure 13: Evolution of semi-major axis a, eccentricity ϵ, longitude of periapsis Φ of a test particle and resonance argument $\varphi = 2\lambda_{\text{Jupiter}} - \lambda_{\text{test}} - \Phi_{\text{st}}$ over a timespan of $t_{\text{sim}} = 100 \cdot T_{\text{Jupiter}} = 1186$ y, for the simulations ($\Delta t = 0.1$ y) of the restricted three-body problem (the Sun, Jupiter and the test particle) with initial values for a, ϵ and Φ as given per figure (a) – (f) in Table 4. Each plot shows the simulations with fixed Sun and $a^0 = a^0_{\text{hcf}}$ (black), fixed Sun and $a^0 = a^0_{\text{comf}}$ (blue), dynamic Sun and $a^0 = a^0_{\text{hcf}}$ (grey), and dynamic Sun and $a^0 = a^0_{\text{comf}}$ (orange). The initial values are chosen such that the test particle and Jupiter are (in the vicinity of) a 2:1 resonance. Jupiter is in a circular orbit ($\epsilon^0_{\text{Jupiter}} = 10^{-5}$ and $\varpi^0_{\text{Jupiter}}$, $\Omega^0_{\text{Jupiter}} = 0$) and is in the same plane as the test particle ($I_{\text{Jupiter}} = I_{\text{test}} = 10^{-4}$ deg). For both Jupiter and the test particle, $\lambda^0 = 0$. The vertical axis ranges are: $[0.60 \cdot a_{\text{Jupiter}}, 0.67 \cdot a_{\text{Jupiter}}]$ for a, $[0, 0.24]$ for ϵ, $[0, 2\pi]$ for Φ and $[-\pi, \pi]$ for φ. Observe that the high-frequency oscillations, most evident in the semi-major axis plots, have the same period as Jupiter's orbital period.

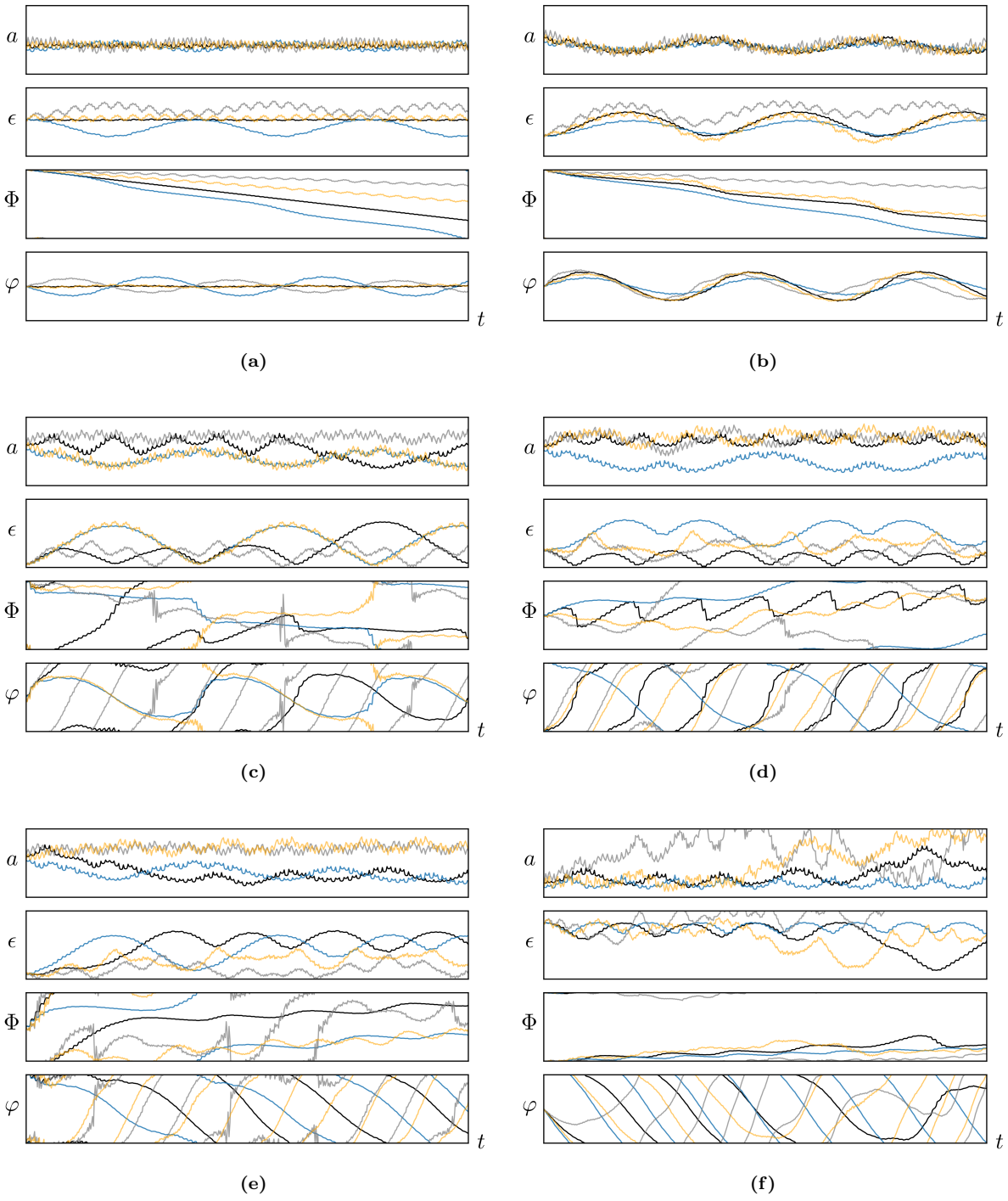

Figure 14: Evolution of semi-major axis a, eccentricity ϵ, longitude of periapsis Φ of a test particle and resonance argument ϕ over a timespan of $t_{\text{sim}} = 100 \cdot T_{\text{Jupiter}} = 1186$ y, for the same simulations as in Figure 13, except with $\Delta t = 2.5$ y. The vertical axis ranges are: $[0.60 \cdot a_{\text{Jupiter}}, 0.67 \cdot a_{\text{Jupiter}}]$ for a, $[0, 0.24]$ for ϵ, $[0, 2\pi]$ for Φ and $[-\pi, \pi]$ for φ.

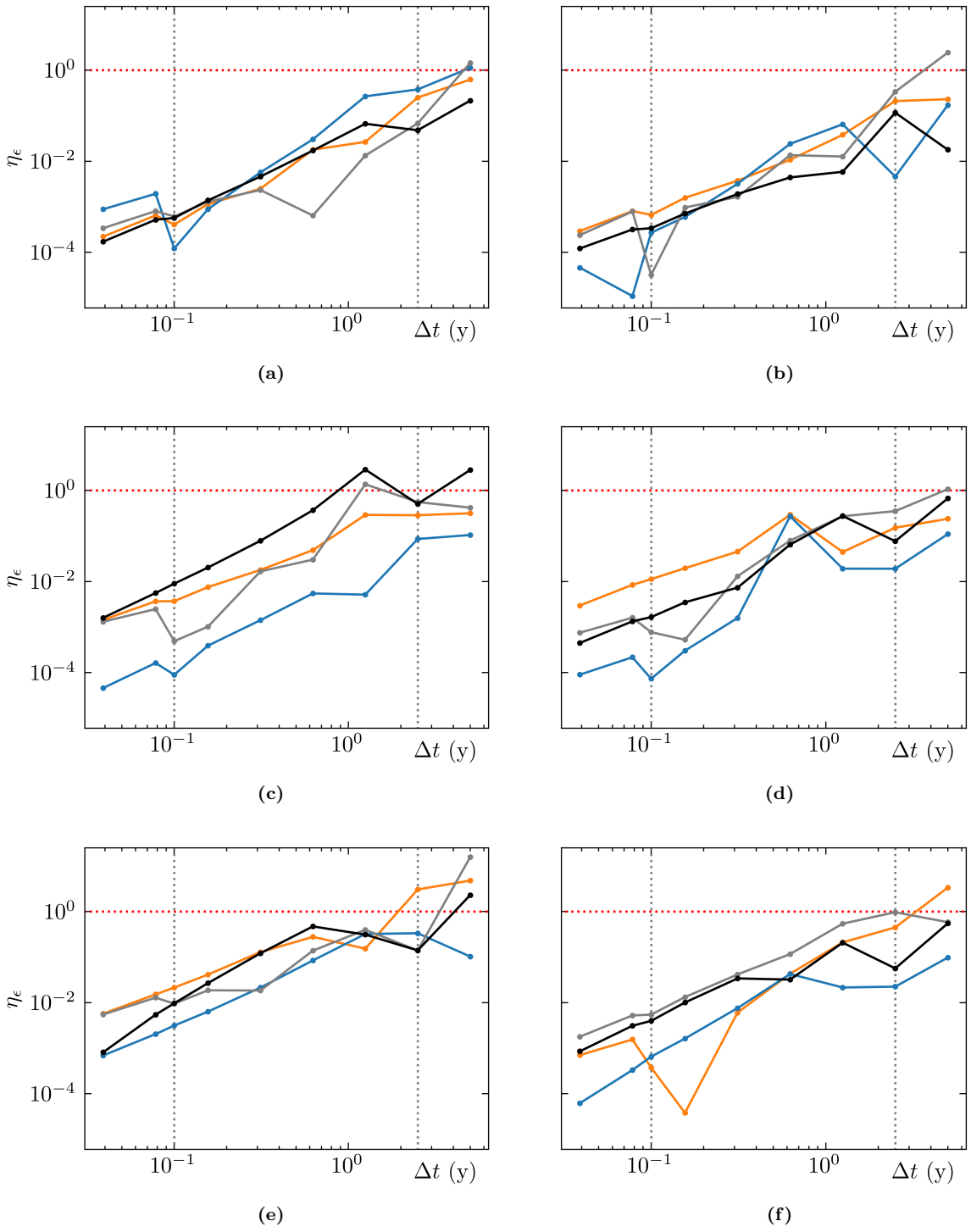

Figure 15: Relative error $\eta_\epsilon = |\epsilon - \epsilon_{\text{ref}}|/\epsilon_{\text{ref}}$ of the test particle's eccentricity as a function of time step Δt, with $\Delta t_{\text{ref}} = 0.01$ y, for the same simulations as in Figures 13 and 14. The points at which $\Delta t = 0.1$ y and $\Delta t = 2.5$ y, the time steps used for the Figures 13 and 14, respectively, are indicated by a grey dotted line. The point at which the relative error $\eta_\epsilon = 1$ is indicated with a red dotted line.

4 Conclusion

We present an implementation of the Wisdom-Holman integrator for simulating systems with N orbiting bodies and a dominant central mass, which models orbits around the (fixed) central mass as Kepler orbits, while gravitational interactions between non-central bodies and the central body motion are modelled as weak perturbations. We explore the possibility of reducing runtime by taking time steps larger than used conventionally, including time steps $\Delta t > T_i$ for at least one body i. To ensure the model correctly describes a two-body system, we introduce for each body i the effective central mass $m_{ci}^* = m_c/(1+\mu_i)^2$, with $\mu_i = m_i/m_c$. Furthermore, we present two methods for advancing a body along its Kepler orbit: Method A, which uses both the Kepler and Cartesian coordinates, changing coordinates each iteration, and Method B, which uses the f and g functions to remain in the Cartesian coordinates.

Simulations with Method B yield slightly larger errors than those using Method A. However, since the difference in magnitude of these two errors remains minimal, and since the relative error of Method B does not exceed 10^{-10}, Method B promises to be the preferred method due to it outperforming Method A computationally (provided that the number of iterations in which the data are stored is limited).

For simulations of the Solar System, consisting of the nine planets (including Pluto), with the Sun fixed at the origin and with the Sun having dynamic position and velocity (i.e. the centre of mass fixed at the origin), the relative error η_ϵ grows as $\mathcal{O}(\Delta t)$ whenever $\Delta t < T$. For simulations of the Solar system with a dynamic Sun, the error becomes too big for time steps $\Delta t \gtrsim T$, resulting in unbounded orbits. Specifically, for the maximum value of the step size $\Delta t_{\max}$ possible such that the numerical stability is preserved, we have that $T_{\text{Mercury}}/\Delta t_{\max} = 6.2$. This agrees with the step size limit according to Viswanath (2002), which is one-sixth of Mercury's orbital period. Fixed Sun simulations are better behaved for $\Delta t > T$ compared to dynamic Sun simulations, with the relative error still equal to $\mathcal{O}(\Delta t)$, which is especially the case for the inner orbits. Although simulations with large time steps can introduce significant errors and may not accurately describe a system for certain applications, they can still provide valuable qualitative information about the system's evolution on long time scales.

The large errors of the dynamic Sun simulations become apparent when considering the magnitudes of the individual components of the Hamiltonian of the system. While the interplanetary interaction Hamiltonian remains minimal compared to the Kepler Hamiltonian, this is not the case for the perturbation Hamiltonian (for the inner planets) that models the motion of the central body. However, due to Jupiter's large mass, this is possibly specific to the Solar System, and planetary systems without the most massive planet in an outer orbit may be more stable for large time steps as well.

The simulation method is tested for its fidelity using both energy conservation and the extent to which it can describe resonance. Results show that the dynamic Sun simulation accurately describes the Solar System and the restricted three-body problem for small time steps ($\Delta t \ll T_i$ for all bodies i). This suggests that the use of Jacobian Coordinates is not strictly necessary, contrary to what is commonly assumed, for example, in Murray & Dermott (2009). For larger time steps, including time steps exceeding the orbital period of planets, fixed Sun simulations still conserve energy to a significant degree, suggesting that qualitative behaviour is maintained when using larger time steps.

Overall, simulations of the Solar System with a fixed Sun can be used with large time steps to obtain the qualitative behaviour of the system. For small step sizes, dynamic Sun simulations accurately describe the Solar System and the restricted three-body problem without the use of Jacobian coordinates. However, for simulations of the Solar System, the step size is limited by $\Delta t_{\max} = T_{\text{Mercury}}/6$. Potential further research includes investigating possible applications for large time step simulations, such as the study of the formation of the Solar System, or any other planetary system. Moreover, investigating other, more statistical means of orbit averaging with large time steps could result in more accurate simulations. Finally, the number of bodies could be extended to include the many asteroids in the Solar System. Since collisions or near-encounters are more probable in this case, taking this into account, for instance, by using the method described in Visser (2023), may need to be taken into consideration.

References

Murray, C. D., & Dermott, S. F. (2009). *Solar system dynamics*. Cambridge University Press.

Süli, E., & Mayers, D. F. (2003). *An introduction to numerical analysis*. Cambridge University Press.

Taylor, J. R. (2005). *Classical mechanics*. University Science Books.

Thijsen, J. (2007). *Computational physics*. Cambridge University Press.

van der Ven, J. R. (2025). Simulationcode. https://github.com/Jimvdv/SimulationCode

Visser, P. M. (2023). Collision detection for n-body kepler systems. *Astronomy & Astrophysics*, *669*, A97. https://doi.org/10.1051/0004-6361/202243754

Viswanath, D. (2002). How many timesteps for a cycle? analysis of the wisdom-holman algorithm. *Bit Numerical Mathematics*.

Williams, D. R. (2016). Planetary fact sheets [Accessed: 23-04-2025].

Wisdom, J., & Holman, M. (1991). Symplectic maps for the n-body problem. *The Astronomical Journal*, *102*, 1528–1538. https://doi.org/10.1086/115978

Appendix A

For a body in a Kepler orbit, the vectors $\mathbf{r}$ and $\mathbf{v}$ span the orbital plane (note that $|\mathbf{r} \times \mathbf{v}| = L/m \neq 0$). We exploit this fact to derive time-dependent expressions for the position and velocity when their values are known for one point on the orbit. Let $\mathbf{r}^0$ and $\mathbf{v}^0$ be the position and velocity vectors at some time t^0. For the position we write

$$\mathbf{r}(t) = f(t, t^0)\mathbf{r}^0 + g(t, t^0)\mathbf{v}^0, \tag{A.1}$$

with f and g functions that depend on time t. The velocity is readily obtained by differentiation, giving us

$$\mathbf{v}(t) = \dot{f}(t, t^0)\mathbf{r}^0 + \dot{g}(t, t^0)\mathbf{v}^0. \tag{A.2}$$

Taking the cross products with $\mathbf{v}^0$ and $\mathbf{r}^0$ on both sides of Equation (A.1), we obtain

$$\mathbf{v}^0 \times \mathbf{r}(t) = -f(t, t^0)\frac{\mathbf{L}}{m} \qquad \text{and} \qquad \mathbf{r}^0 \times \mathbf{r}(t) = g(t, t^0)\frac{\mathbf{L}}{m}. \tag{A.3}$$

We can get a useful expression for f and g by employing Equations (2.20) and (2.22). Without loss of generality, we assume the rotation matrix is the identity matrix and so

$$\begin{aligned}
\mathbf{v}^0 \times \mathbf{r}(t) &= \frac{\omega a^2 b}{r^0}\left[-\sin E^0 \sin E - \cos E^0 \cos E + \epsilon \cos E^0\right]\mathbf{k} \\
&= \frac{\omega a^2 b}{r^0}\left[-\cos(E - E^0) + \epsilon \cos E^0\right]\mathbf{k} \\
&= \frac{\omega a^2 b}{r^0}\left[-\cos(\Delta E) + \epsilon \cos E^0\right]\mathbf{k},
\end{aligned}$$

with $\Delta E = E - E^0$, the difference between the eccentric anomalies at positions $\mathbf{r}(t)$ and $\mathbf{r}^0$. Equating the z-coordinates in Equation (A.3), and using Equation (2.3) and the fact that $\mathbf{L} = (m\omega ab)\mathbf{k}$, it follows that

$$f(t, t^0) = 1 - \frac{a}{r^0}\left(1 - \cos \Delta E\right). \tag{A.4}$$

Similarly,

$$\mathbf{r}^0 \times \mathbf{r}(t) = ab\left[\sin \Delta E - \epsilon(\sin E - \sin E^0)\right]\mathbf{k}$$

or, using Equation (2.8) with $\Delta t = t - t^0$,

$$\mathbf{r}^0 \times \mathbf{r}(t) = ab\left[\sin \Delta E + (\omega \Delta t - \Delta E)\right]\mathbf{k}.$$

Again, equating z-coordinates in (A.3), we get

$$g(t, t^0) = \Delta t - \frac{1}{\omega}(\Delta E - \sin \Delta E). \tag{A.5}$$

By Equation (2.21)

$$\frac{\mathrm{d}}{\mathrm{d}t}(\Delta E) = \frac{\mathrm{d}E}{\mathrm{d}t} = \frac{\omega a}{r},$$

and so it follows that

$$\dot{f}(t, t^0) = -\frac{a^2 \omega}{r r^0}\sin \Delta E \tag{A.6}$$

and

$$\dot{g}(t, t^0) = 1 - \frac{a}{r}(1 - \cos \Delta E). \tag{A.7}$$

Note that f and g (and their derivatives) depend only on Δt and ΔE, with the latter also depending only on Δt according to Equation (2.9). Hence, we write $f(t, t^0) = f(\Delta t)$ and $g(t, t^0) = g(\Delta t)$.

Appendix B

Here, we derive Equation (2.9). The goal is to find an equation that expresses the time difference $\Delta t = t^1 - t^0$ in terms of the difference of eccentric anomalies $\Delta E = E^1 - E^0$. We first evaluate the cross product $\boldsymbol{\epsilon} \times \Delta \mathbf{r}$, with $\Delta \mathbf{r} = \mathbf{r}^1 - \mathbf{r}^0$. Without loss of generality we assume that the angles ϖ, Ω and I are all equal to 0 because the rotation matrix preserves cross products, i.e. $(\mathscr{R}\mathbf{a}) \times (\mathscr{R}\mathbf{b}) = \mathscr{R}(\mathbf{a} \times \mathbf{b})$. With $\boldsymbol{\epsilon}$ and $\Delta \mathbf{r}$ given by

$$\boldsymbol{\epsilon} = \epsilon \begin{pmatrix} 1 \\ 0 \\ 0 \end{pmatrix} \quad \text{and} \quad \Delta \mathbf{r} = \begin{pmatrix} a \cos E^1 - a \cos E^0 \\ b \sin E^1 - b \sin E^0 \\ 0 \end{pmatrix},$$

we get that

$$\boldsymbol{\epsilon} \times \Delta \mathbf{r} = b(\sin E^1 - \sin E^0)\mathbf{k}.$$

Combining this with Equation (2.8) gives us

$$\Delta E - \omega \Delta t = \epsilon(\sin E^1 - \sin E^0) = \frac{1}{b} |\boldsymbol{\epsilon} \times \Delta \mathbf{r}| = \frac{\boldsymbol{\epsilon} \times \Delta \mathbf{r}}{b} \cdot \frac{\mathbf{L}}{L}, \tag{B.1}$$

where the last equality follows from the fact that $\mathbf{L}/L$ is a unit vector pointing in the direction of $\boldsymbol{\epsilon} \times \Delta \mathbf{r}$. We want to eliminate the dependence of $\mathbf{r}^1$ because the new position is still unknown. We achieve this using the f and g functions defined in Equation (A.1). Equation (B.1) can then be written as

$$\Delta E - \omega \Delta t = (f - 1)\frac{\boldsymbol{\epsilon} \times \mathbf{r}^0}{b} \cdot \frac{\mathbf{L}}{L} + g\frac{\boldsymbol{\epsilon} \times \mathbf{v}^0}{b} \cdot \frac{\mathbf{L}}{L}.$$

We now use Equation (2.15) to eliminate $\boldsymbol{\epsilon}$. First note that

$$\begin{aligned}
(\boldsymbol{\epsilon} \times \mathbf{r}^0) \cdot \mathbf{L} &= \left[\left(\frac{\mathbf{v}^0 \times \mathbf{L}}{G m_c m} - \frac{\mathbf{r}^0}{r} \right) \times \mathbf{r}^0 \right] \cdot \mathbf{L} \\
&= \frac{(\mathbf{v}^0 \times \mathbf{L}) \times \mathbf{r}^0}{G m_c m} \cdot \mathbf{L} \\
&= \frac{\mathbf{L}(\mathbf{r}^0 \cdot \mathbf{v}^0) - \mathbf{v}^0(\mathbf{r}^0 \cdot \mathbf{L})}{G m_c m} \cdot \mathbf{L} \\
&= \frac{\mathbf{r}^0 \cdot \mathbf{v}^0}{G m_c m} L^2,
\end{aligned}$$

since $\mathbf{r}^0 \times \mathbf{r}^0 = \mathbf{0}$ and $\mathbf{r}^0 \cdot \mathbf{L} = 0$. Similarly, we have

$$(\boldsymbol{\epsilon} \times \mathbf{v}^0) \cdot \mathbf{L} = \frac{(v^0)^2 L^2}{G m_c m} - \frac{L^2}{m r^0},$$

and hence

$$\Delta E - \omega \Delta t = (f-1)\frac{(\mathbf{r}^0 \cdot \mathbf{v}^0)L}{Gm_c mb} + g\frac{(v^0)^2 L}{Gm_c mb} - g\frac{L}{mr^0 b}$$

$$= (f-1)\frac{\mathbf{r}^0 \cdot \mathbf{v}^0}{\omega a^2} + g\frac{(v^0)^2}{\omega a^2} - g\frac{\omega a}{r^0},$$

where the last equality from $Gm_c = \omega^2 a^3$ and $L = m\omega ab$. Next, we use the vis-viva equation

$$(v^0)^2 = Gm_c\left(\frac{2}{r^0} - \frac{1}{a}\right) = \omega^2 a^2\left(\frac{2a}{r^0} - 1\right), \tag{B.2}$$

which can be derived from energy conservation (Murray & Dermott 2009), and arrive at

$$\Delta E - \omega \Delta t = (f-1)\frac{\mathbf{r}^0 \cdot \mathbf{v}^0}{\omega a^2} + g\omega\left(\frac{a}{r^0} - 1\right)$$

Lastly, we substitute the expressions for the f and g functions (Eqs. (A.4) and (A.5)) into the above, which, after rewriting, results in

$$\Delta E - \omega \Delta t = (\cos \Delta E - 1)\,\frac{\mathbf{r}^0 \cdot \mathbf{v}^0}{\omega a^2} + \left(1 - \frac{r^0}{a}\right)\sin \Delta E.$$

Appendix C

Table 5: Fit parameters α (slope) and β (offset) for the numerical fits in Figures 9 and 10. The logarithmic values of the data points are fitted with a linear function, i.e. the fits are of the form $\ln \eta = \alpha \ln \Delta t + \beta$, with η the (relative) error and Δt the time step. Parameters with subscript *fixed* are for data points obtained from simulations with a fixed Sun (depicted in black in the figures), and parameters with subscript *dynamic* are for data points obtained from simulations with a dynamic Sun (depicted in blue in the figures).

Figure	α_{fixed} (black)	β_{fixed} (black)	α_{dynamic} (blue)	β_{dynamic} (blue)
9(a)	1.28 ± 0.06	-30.2 ± 7	0.8 ± 0.1	-15 ± 1
9(b)	1.03 ± 0.03	-23.1 ± 0.4	1.10 ± 0.4	-20.0 ± 0.5
9(c)	1.08 ± 0.02	-25.0 ± 0.3	1.11 ± 0.04	-23.3 ± 0.4
9(d)	1.05 ± 0.02	-23.5 ± 0.3	1.11 ± 0.04	-25.3 ± 0.4
10(a)	0.86 ± 0.07	-21 ± 1		
10(b)	0.98 ± 0.09	-23 ± 2		
10(c)	0.87 ± 0.07	-20 ± 1		
10(d)	1.05 ± 0.06	-24 ± 1		